LA-UR-11-11271
Approved for public release; distribution is unlimited.

Title: ENDF/B-VII.1 Neutron Cross Section Data Testing with Critical Benchmark Assemblies

Author(s):
Kahler, Albert C
Arcilla, Ramon
Chadwick, Mark B
Dunn, Michael E
Gouw, Reza R
Herman, Michal
Hiruta, Hikaru
Kiedrowski, Brian C
Lell, Richard M
MacFarlane, Robert E
McKnight, Richard D
Mosteller, Russell D
Palmiotti, Giuseppe
Sublet, Jean-Christophe
Trkov, Andre
Trumbull, Timothy H
Zerkle, Michael L

Intended for: Nuclear Data Sheets

ENDF/B-VII.1 Neutron Cross Section Data Testing with Critical Assembly Benchmarks

A. C. Kahler[1,*], R. E. MacFarlane[1], R. D. Mosteller[1], B. C. Kiedrowski[1],M. B. Chadwick[1], R. D. McKnight[2], R. M. Lell[2], G. Palmiotti[3], H. Hiruta[3], M. Herman[4], R. Arcilla[4], J. C. Sublet[5], A. Trkov[6], M. Dunn[7], T. H. Trumbull[8], M.L. Zerkle[9], R. R. Gouw[9]

[1] *Los Alamos National Laboratory, Los Alamos, NM 87545, USA*
[2] *Argonne National Laboratory, Argonne, IL 60439, USA*
[3] *Idaho National Laboratory, Idaho Falls, Id 83415, USA*
[4] *Brookhaven National Laboratory, Upton, NY 11973, USA*
[5] *Culham Centre for Fusion Energy, Abingdon, OX14 3DB, UK*
[6] *Jozef Stefan Institute, Jamova 39, 1000 Ljubljana, Slovenia*
[7] *Oak Ridge National Laboratory, Oak Ridge, TN 37831, USA*
[8] *Knolls Atomic Power Laboratory, Schenectady, NY 12309, USA*
[9] *Bettis Atomic Power Laboratory, West Mifflin, Pa 15122, USA*

(Received August 9, 2011)

The ENDF/B-VII.1 library is the latest revision to the United States' Evaluated Nuclear Data File (ENDF). The ENDF library is currently in its seventh generation, with ENDF/B-VII.0 being released in 2006. This revision expands upon that library, including the addition of new evaluated files (was 393 neutron files previously, now 418 including replacement of elemental vanadium and zinc evaluations with isotopic evaluations) and extension or updating of many existing neutron data files. Complete details are provided in the companion paper. This paper focuses on how accurately application libraries may be expected to perform in criticality calculations with these data. Continuous energy cross section libraries, suitable for use with the MCNP Monte Carlo transport code, have been generated and applied to a suite of nearly one thousand critical benchmark assemblies defined in the International Criticality Safety Benchmark Evaluation Project's International Handbook of Evaluated Criticality Safety Benchmark Experiments. This suite covers uranium and plutonium fuel systems in a variety of forms such as metallic, oxide or solution, and under a variety of spectral conditions, including unmoderated (i.e., bare), metal reflected and water or other light element reflected. Assembly eigenvalues that were accurately predicted with ENDF/B-VII.0 cross sections such as unmoderated and uranium reflected ^{235}U and ^{239}Pu assemblies, HEU solution systems and LEU oxide lattice systems that mimic commercial PWR configurations continue to be accurately calculated with ENDF/B-VII.1 cross sections, and deficiencies in predicted eigenvalues for assemblies containing selected materials, including titanium and tungsten are greatly reduced. Other deficiencies, such as the overprediction of Pu solution system critical eigenvalues and a decreasing trend in calculated eigenvalue for ^{233}U fueled systems as a function of Above-Thermal Fission Fraction remain. The comprehensive nature of this critical benchmark suite and the generally accurate calculated eigenvalues obtained with ENDF/B-VII.1 neutron cross sections support the conclusion that this is the most accurate general purpose ENDF/B cross section library yet released to the technical community.

[*]) Corresponding author, electronic address: akahler@lanl.gov

Contents

I. Introduction

The ENDF/B-VII.1 cross section library represents the latest advance in the United States' evaluated nuclear data file. This library builds upon the ENDF/B-VII.0 library that was released in 2006 [1]. Improvements in basic nuclear data that are embodied in this new library are discussed in the companion article to this paper [2]. This paper expands upon that report to describe how these new data perform when used in a Monte Carlo application

library. Application libraries have been independently created with the NJOY Nuclear Data Processing System [3] by several of the co-authors and subsequently used with the continuous energy Monte Carlo MCNP code [4], in a variety of calculations to test the accuracy of the underlying nuclear data. These calculations are described below.

A broad outline of this paper begins with an overview of application library generation; a process used for all 418 of the ENDF/B-VII.1 neutron files whether they appear in a subsequent benchmark model calculation or not. The majority of data testing performed herein utilize critical benchmark models defined in the International Criticality Safety Benchmark Evaluation Project (ICSBEP) Handbook [5]. Additional calculations to predict measured reaction rate measurements are also documented. These criticality calculations provide a broad test of the underlying nuclear data, as they involve a variety of fuel (fissile) nuclides under a variety of conditions (bare, moderated, and reflected). Specific benchmark attributes are given in subsequent sections.

There are notable improvements in selected benchmarks with ENDF/B-VII.1 cross sections compared to use of ENDF/B-VII.0 cross sections. Among these are reflected systems containing significant quantities of titanium and tungsten. Resolution of other long-standing bias', such as the historical overprediction of Pu solution system eigenvalues remain for a future ENDF release. Details of the successes, both new and continuing, for the ENDF/B-VII.1 library follow.

II. Data Testing

Critical eigenvalue calculations, and in selected instances, reaction rate calculations have been performed for nearly one thousand critical benchmark assemblies. It is neither practical, nor necessary, to describe these benchmarks in detail, nor to analyze the calculated results of every benchmark in order to assess the ENDF/B-VII.1 cross section library. Rather, this section is divided into logical partitions that describe (i) the processing of these data into an application library for MCNP with NJOY; (ii) an overview of the International Criticality Safety Benchmark Evaluation Project Handbook for which most of the benchmarks are described; (iii) several sections of benchmarks grouped by common attributes such as spectrum or fuel type; (iv) specialized calculations that yield C/E results for reaction rates or Rossi-a.

A. NJOY Processing

The NJOY Nuclear Data Processing System has been used to create ACE formatted files for all 418 neutron evaluations of the ENDF/B-VII.1 library. While significant additional quality checks are needed before such files are formally released to the broader technical community, sufficient internal checking has been done to allow their use in the validation calculations of ICSBEP benchmarks with MCNP that follow.

NJOY is a modular program, with a variety of subprograms each performing a unique task in a multistep sequence that starts from the original ENDF-formatted file and ends with an ACE file suitable for use in an MCNP calculation. The ENDF/B-VII.1 files processed here used NJOY's "RECONR", "BROADR", "UNRESR", "HEATR", "PURR", GASPR" and "ACER" modules. RECONR is used to create a unionized energy grid for all cross sections of a given evaluated file. If resolved resonance parameters are present, they are expanded into the appropriate pointwise cross sections, typically scattering, capture and possibly fission. Also, with the Limited Reich-Moore (LRF=7) format, there may be resonant charged particle and/or inelastic scattering cross sections. In the ENDF/B-VII.1 library there are two evaluated files, ^{19}F and ^{35}Cl that use the LRF=7 format. Linear interpolation is used for intervening energy points, and the density of energy points is sufficient to assure that this interpolation is accurate to within a user specified tolerance. For the files generated herein that tolerance is 0.1%. The output from RECONR is passed to BROADR, where the cross sections are Doppler broadened to 293.6 °K. NJOY allows the user to specify a different linear interpolation tolerance as part of its BROADR input, but in most instances (including here) we choose to maintain the same linear interpolation tolerance as used in RECONR. UNRESR and HEATR which follow are not necessarily needed for the MCNP transport calculations performed herein, but they are important and necessary steps to create a complete processed file and so we include these steps in our generic NJOY processing. PURR is used to create unresolved resonance probability tables. Our standard PURR job uses 32 probability bins and computes 64 ladders. GASPR is used to accumulate the various cross sections that produce charged particles (p, d, t, 3He and α) into a single cross section. It is not necessary for transport calculations, but is often used for calculating production of the particle of interest. Finally, ACER is used to accumulate the various quantities into MCNP's ACE format.

B. ICSBEP Benchmark Overview

As noted in the Introduction, the vast majority of benchmark results presented herein come from models defined by the International Criticality Safety Benchmark Evaluation Project, as defined in the International Handbook of Evaluated Criticality Safety Benchmark Experiment. Evaluations in this Handbook are defined using an XXX-YYY-ZZZ-aaa.b nomenclature system. The XXX designator defines the fuel system and includes Pu for ^{239}Pu fueled systems, and HEU, IEU and LEU for highly-enriched, intermediate-enriched and low-enriched ^{235}U fuel systems. Highly enriched systems contain at least 90% ^{235}U, low-enriched systems contain less than 10% ^{235}U while intermediate-enriched systems cover the intervening range. Other XXX designators include U233 for ^{233}U fueled systems and "MIX" which is used for

systems with both ^{235}U and ^{239}Pu. The YYY designator defines the chemical form of the fuel, with MET meaning a metal system, SOL being a solution and COMP a compound. ZZZ is used to define the average fission energy. FAST is used when more than 50% of the fissions occur above 100 keV and THERM is used if more than 50% of the fissions occur below 0.625 eV. INTER is used when 50% or more of the fissions occur between these energy limits, and MIXED is used when no energy interval has 50% or more fissions. Finally, ###.a is a simple numerical index, and ".a" represents one of the individual case numbers when multiple experiments are described in a single evaluation. As it can be unwieldy to cite the complete evaluation name, we often can use only the first initial of each designator to uniquely specify a benchmark; for example the HEU-MET-FAST-001 benchmark, is abbreviated HMF1 in this paper.

The ICSBEP Handbook contains hundreds of evaluated experiments, representing several thousand critical configurations. The Handbook is re-issued annually and usually contains several dozen new experiments in each issue. It is neither necessary, nor practical, to perform calculations for all of these benchmarks to validate the ENDF/B-VII.1 library. However, over the years we have created MCNP models for nearly one thousand of these benchmarks. Many are discussed in the ensuing sections, and we summarize the calculated eigenvalues for all of them in the Appendix.

One particularly valuable aspect of the Handbook is the occurrence of many related experiments that utilize similar or identical materials with only small changes. While the information gleaned from analyzing any individual experiment is valuable in its own right, the added information obtained from extracting correlated information over a wider range of parameters allows one to have greater confidence in the resulting conclusions about the accuracy of the underlying nuclear data and its overall range of applicability. The HMF7 experiment is one such example. These experiments were performed at Oak Ridge National Laboratory (ORNL) and utilize the same fuel material, but include varying amounts of polyethylene. This series of experiments, while categorized as "FAST" actually has an average fission energy that varies from ~830 keV to a low of ~34 eV. Naturally the flux and fission production distributions span broad distribution of energies about the average for each of these assemblies, but the wide average energy range spanned by these measurements provides an important test of the underlying cross section data. Another example is the suite of experiments scattered throughout the HEU-MET-FAST and HEU-MET-MIXED categories from RFNC-VNIITF (Russian Federal Nuclear Center at the All-Russian Institute of Technical Physics) that use the same HEU fuel plates but include a variety of materials placed as axial reflectors, axial and radial reflectors or as diluent material placed between individual HEU slabs. Among the non-fissile materials used are aluminum, titanium, vanadium, iron and tungsten. These experiments include increasing amounts of the various materials in an axial reflector configuration, or various combinations of these materials and polyethylene. Again we have multiple arrangements with a common fuel material that then allows for testing the cross section adequacy of the substituted materials over a wide range of some parameter such as average fission energy or material thickness. ICSBEP users will quickly find other examples.

C. Fast Systems

The historical Los Alamos National Laboratory suite of FAST experiments represents a simple subset of the ICSBEP FAST benchmark category that is easily calculated to obtain an initial indication of the high energy cross section data for the important uranium and plutonium nuclides. These experiments include Godiva (HMF1), Flattop (HMF28), Jezebel and "dirty" Jezebel (PMF1, PMF2), Flattop-Pu (PMF6), Thor (PMF8), Big-10 (IMF7), plus Jezebel-23 and Flattop-23 (UMF1, UMF6). Details of these assemblies are summarized in Table 1.

Table 1. Attributes of traditional LANL critical assemblies and their corresponding ICSBEP Benchmark Name.

ICSBEP Bench-mark	Tradi-tional Name	Geometry	Material
HMF1	Godiva	Bare Sphere	HEU
HMF28	Flattop	Reflected Sphere	HEU (core) ^{nat}U (refl)
PMF1 PMF2	Jezebel "dirty" Jezebel	Bare Sphere	^{239}Pu+4.5 a/o ^{240}Pu ^{239}Pu+20.1 a/o ^{240}Pu
PMF6	Flattop-Pu	Reflected Sphere	^{239}Pu (core) ^{nat}U (refl)
PMF8	Thor	Reflected Sphere	^{239}Pu (core) ^{232}Th (refl)
IMF7	Big-10	Cylinder	Heterogeneous mix of uranium plates with varying ^{235}U content
UMF1	Jezebel -23	Bare Sphere	^{233}U
UMF6	Flattop-23	Reflected Sphere	^{233}U (core) ^{nat}U (refl)

Calculated eigenvalues with ENDF/B-VII.1 cross sections are shown in Fig. 1, below. There are several features of this figure common to many that will appear in this paper. First, the ordinate is commonly labeled "k_{eff} C/E", or perhaps "C/E Value for k_{eff}". This means that the plotted data are the MCNP calculated eigenvalue divided by the expected model eigenvalue. There are innumerable approximations that might cause the model of a critical system to yield a non-unit eigenvalue and so for consistency when comparing multiple benchmarks we normalize the calculated eigenvalues. Also, our MCNP kcode calculations often track 50 million histories, or more

when obtaining reaction rate tallies. This means the stochastic uncertainty on the eigenvalue calculation is often only a few pcm. This uncertainty is comparable to the size of the plotted datum and so we do not include it in our figures. We do however include the experimental reactivity uncertainty that is published in the ICSBEP evaluation. These uncertainties are included in the figures as "error bars" centered on unity. Finally, the ordinate range is often defined as 0.975 to 1.025. The plotted data may be situated much closer to unity, but 5% is an important interval in many safety analyses and we find it informative to illustrate the accuracy of our eigenvalue calculations on such a scale.

For the traditional LANL assemblies, the calculated eigenvalues are all close to unity, and virtually identical to the accurate eigenvalue results obtained previously with ENDF/B-VII.0 cross sections. The only calculated eigenvalue that is clearly outside the experimental uncertainty is the Thor benchmark. The published experimental uncertainty in the ICSBEP Handbook for this benchmark is only 60 pcm, and is likely underestimated as the mass uncertainty that is also given suggests the uncertainty is more likely closer to 150 pcm. The calculated Thor eigenvalue is near 0.998, yielding a C/E value which is only slightly larger than one standard deviation removed from this more realistic uncertainty estimate. Observing virtually no change in calculated eigenvalues with ENDF/B-VII.1 cross sections, compared to those obtained with ENDF/B-VII.0, is expected since only minimal changes to the delayed neutron data (reverting back to the values from ENDF/B-VI.8) have been made for the primary fissile nuclides in ENDF/B-VII.1.

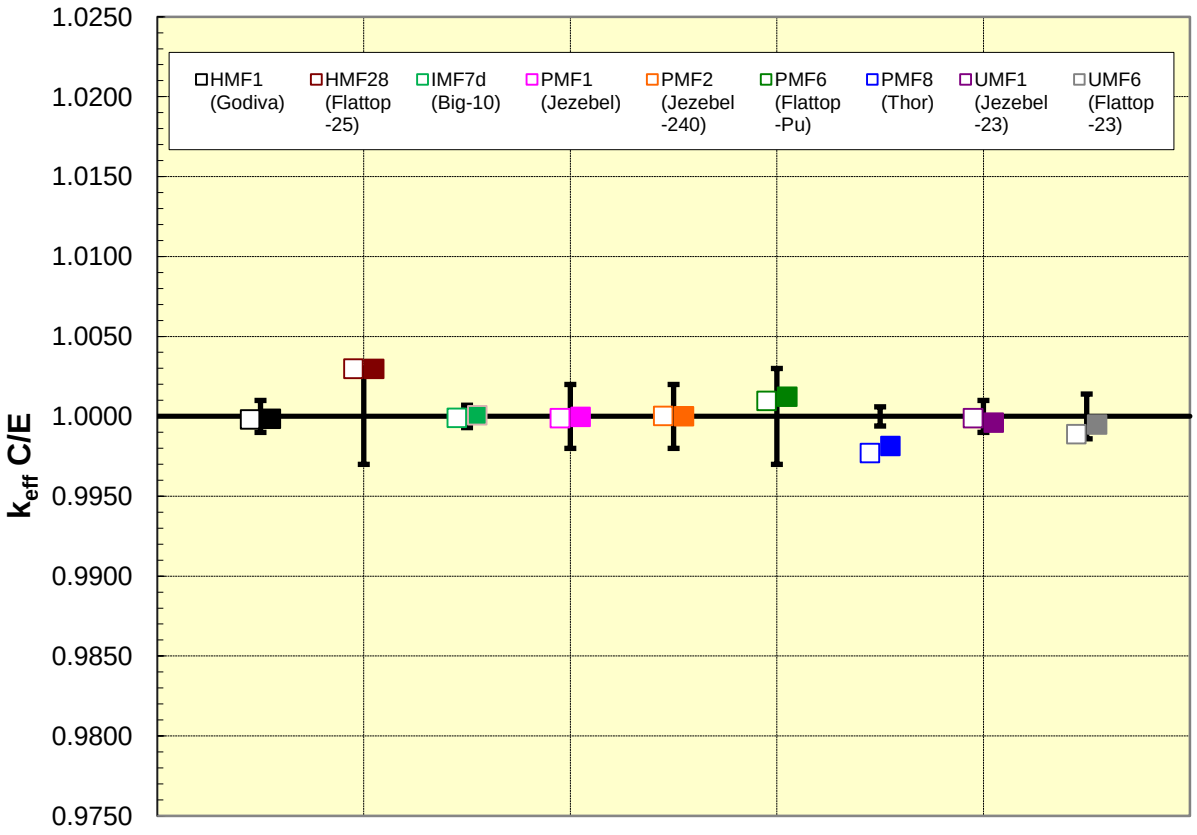

Fig. 1. Calculated Eigenvalues with ENDF/B-VII.0 (closed symbols) and ENDF/B-VII.1 (open symbols) Cross Sections for a Selection of LANL Critical Assemblies. Error bars represent the reported experimental uncertainty.

There are many other FAST system benchmarks for which eigenvalue calculations have been performed. Among these are a series of Russian experiments consisting of a sequence of cylindrical HEU plates approximately 20 cm in diameter and approximately 1 cm tall each. These plates are stacked in two sub-critical assemblies that are moved together to create a critical or near critical assembly. Permutations on these assemblies involve the placement of extra material at the ends of these assemblies (i.e., axial reflectors), placement of extra material between the individual HEU plates (i.e., insertion of diluents or moderators) and further combinations that also include the use of radial reflector material. Various combinations of HEU and these extra materials allow for testing of those extra material's nuclear data. For example, HMF79 consists of five configurations with a central HEU core region and varying thicknesses of Ti axial reflectors (approximately 1 cm, 2 cm, 4 cm, 10 cm and 20 cm thick respectively). The central region consists of ten or eleven HEU plates. Criticality is controlled by

fixing five or six of these plates plus upper reflector in place and slowly moving the near mirror image lower half of the assembly toward the fixed material. Depending upon the specific materials criticality is obtained when the gap between fixed and movable sections is less than a few centimeters, and often only a few millimeters. The average fission energy is little changed in an experiment such as this that only involves heavy materials, but being able to accurately calculate the critical eigenvalue as a function of reflector thickness provides confidence that the high energy scattering cross sections and their associated angular distributions are accurate. A variation of these experiments is to then place the axial reflector material between the individual HEU plates to act as a diluent, or to increase the average energy variation through use a combination of diluents and polyethylene. Some structural materials of interest that have been used in these types of experiments are noted in Table 2.

Table 2. Summary list of fast ICSBEP benchmarks with common fuel plates and varying reflector and/or diluents materials.

Benchmark	Axial Reflector	Diluent	Radial Reflector
HMF15	---	---	---
HMF65	---	---	---
HMF82	CH_2 (top)	---	---
HMF91	CH_2	---	---
HMF44	Al	---	---
HMF89	---	Al	---
HMF34.2	---	Al/CH_2	CH_2
HMF79	Ti	---	---
HMF34.1	---	Ti/CH_2	Ti/CH_2
HMM1	---	Ti/CH_2	Ti/CH_2
HMM15	---	Ti/CH_2	Ti/CH_2
HMF25	V	---	---
HMF40	---	V	---
HMM16	CH_2	V/CH_2	CH_2
HMF43	Fe (steel)	---	---
HMF87	---	Fe (steel)	---
HMF33	---	Fe(steel)/CH_2	---
HMF34.3	---	Fe(steel)/CH_2	---
HMF49	W	---	---
HMF50	---	W	---
HMM17	CH_2	W/CH_2	CH_2

Additional experimental evaluations for these and other materials will be introduced into the ICSBEP Handbook in future years. For example, an experiment similar to HMF89 uses Al as a diluent and also includes both axial and radial polyethylene reflectors has been designated HMF90 and is currently undergoing final review with the expectation of being published in the next edition of the ICSBEP Handbook. Aluminum and iron are two important structural materials noted in the above tabulation of measurements, but there has been little or no change in these cross sections between ENDF/B-VII.0 and ENDF/B-VII.1, and so we expect little change in calculated eigenvalues for HEU benchmarks with only these materials. Such is the case, as shown in the Table 3; the calculated ENDF/B-VII.0 and ENDF/B-VII.1 eigenvalues are nearly identical and close to unity. Also shown in Table 3 is the energy corresponding to the average lethargy causing fission. This is a common measure of the average assembly energy (although the reader is reminded that the actual energy distribution about this average is very broad), and can vary from a high in excess of 800 keV for unmoderated systems to low keV values or eV values depending upon the degree of moderation in any given critical assembly.

Table 3. Calculated eigenvalues for various bare and reflected benchmark assemblies with common fuel plates. Benchmark attributes are summarized in Table 2. Multiple values for selected assemblies indicate differing material arrangements. Refer to the ICSBEP Handbook for details.

Benchmark	ENDF/B-VII.0 k_{eff} C/E *	ENDF/B-VII.0 k_{eff} C/E *	EALF, MeV **
HMF15	0.99510(9)	0.99489(9)	0.831
HMF65	0.99860(9)	0.99852(9)	0.831
HMF82	0.99727(10)	0.99712(10)	0.187
	0.99721(10)	0.99711(10)	0.119
	0.99956(10)	0.99951(10)	0.080
HMF91	1.00002(11)	1.00009(11)	0.0085
HMF44	1.00049(9)	1.00060(9)	0.820
	1.00008(9)	0.99987(9)	0.815
	1.00030(9)	1.00037(9)	0.805
	0.99996(9)	0.99983(9)	0.798
	1.00050(9)	1.00057(9)	0.796
HMF89	1.00102(9)	1.00090(9)	0.771
HMF34.2	0.99949(11)	0.99976(11)	0.0141
HMF43	0.99955(9)	0.99964(9)	0.820
	0.99860(9)	0.99861(9)	0.813
	0.99916(9)	0.99925(9)	0.805
	0.99787(9)	0.99775(9)	0.793
	0.99892(9)	0.99892(9)	0.791
HMF87	0.99989(9)	0.99965(9)	0.751
HMF33	0.99998(11)	0.99993(11)	0.0138
	0.99847(12)	0.99853(12)	0.0019
HMF34.3	0.99843(11)	0.99826(11)	0.0130

* Values in parenthesis represent the uncertainty in the corresponding least significant digits.

** EALF = Energy of average lethargy causing fission. The ENDF/B-VII.1 value is given but the results are virtually identical for ENDF/B-VII.0.

Other materials, most notably titanium and tungsten, have seen significant changes in their cross sections between ENDF/B-VII.0 and ENDF/B-VII.1. These changes were motivated by the large k_{eff} C/E deviations from unity for ENDF/B-VII.0 based calculations. The observed variation in predicted k_{eff} values with recent ENDF/B cross sections is in the Fig. 2.

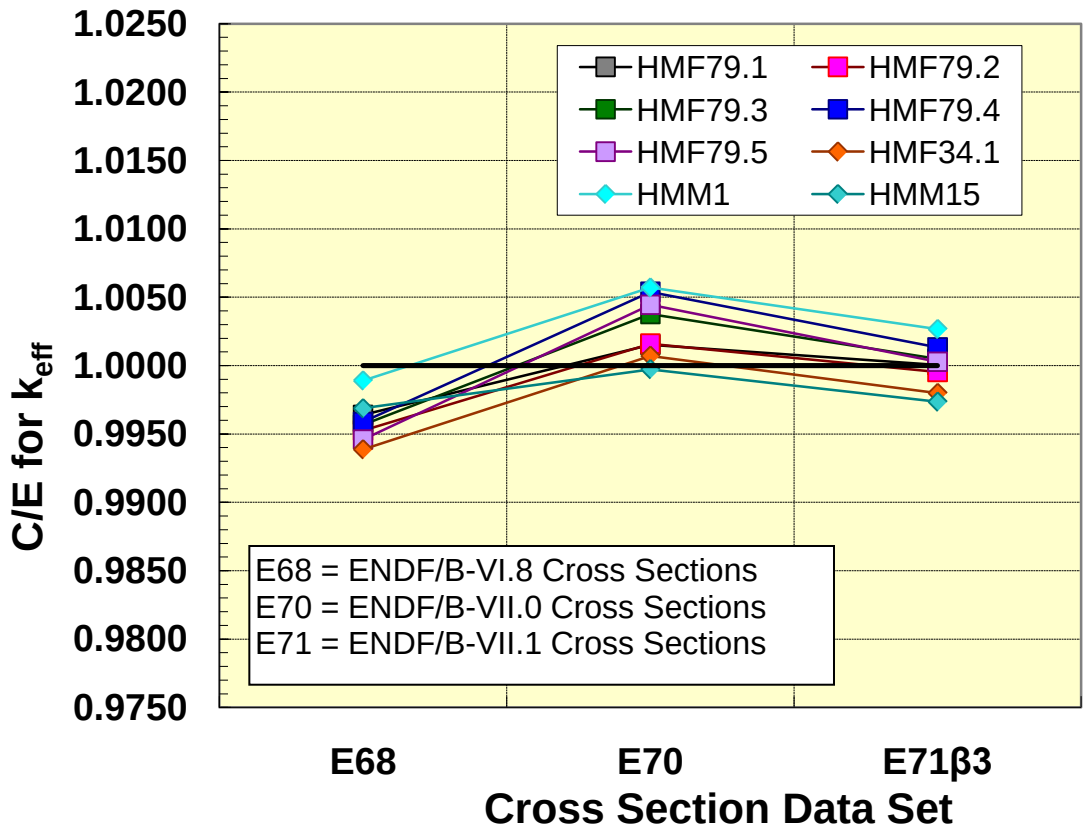

Fig. 2. Calculated Eigenvalues for Titanium Bearing HEU Benchmarks with ENDF/B-VI.8 (E68), ENDF/B-VII.0 (E70) and ENDF/B-VII.1 (E71) Cross Sections.

Measurements have been made for eight assemblies using the same HEU fuel and varying amounts of Ti or a combination of Ti and polyethylene. With ENDF/B-VI.8 cross sections the average calculated eigenvalue is too low by just over 400 pcm and there is a 500 pcm variation from the minimum to maximum calculated eigenvalue; a result that is actually better than it might first appear as the bare ENDF/B-VI HEU calculated eigenvalues were also biased low by ~0.2%. However, with ENDF/B-VII.0 cross sections the average calculated eigenvalue is too large by almost 300 pcm, there appears to be a systematic increase of nearly 400 pcm in calculated eigenvalue with increasing reflector thickness and there is a 600 pcm variation from the minimum to maximum calculated eigenvalue. Clearly the cross section changes embodied in moving from ENDF/B-VI.8 to ENDF/B-VII.0 did not yield an improvement in critical eigenvalue calculations for Ti bearing systems. With ENDF/B-VII.1 cross sections the average eigenvalue is virtually unity and the eigenvalue trend with reflector thickness has been reduced by nearly 50%. The overall minimum to maximum variation, now 530 pcm, remains large. Fig. 3 illustrates these same calculated eigenvalues, now plotted against EALF.

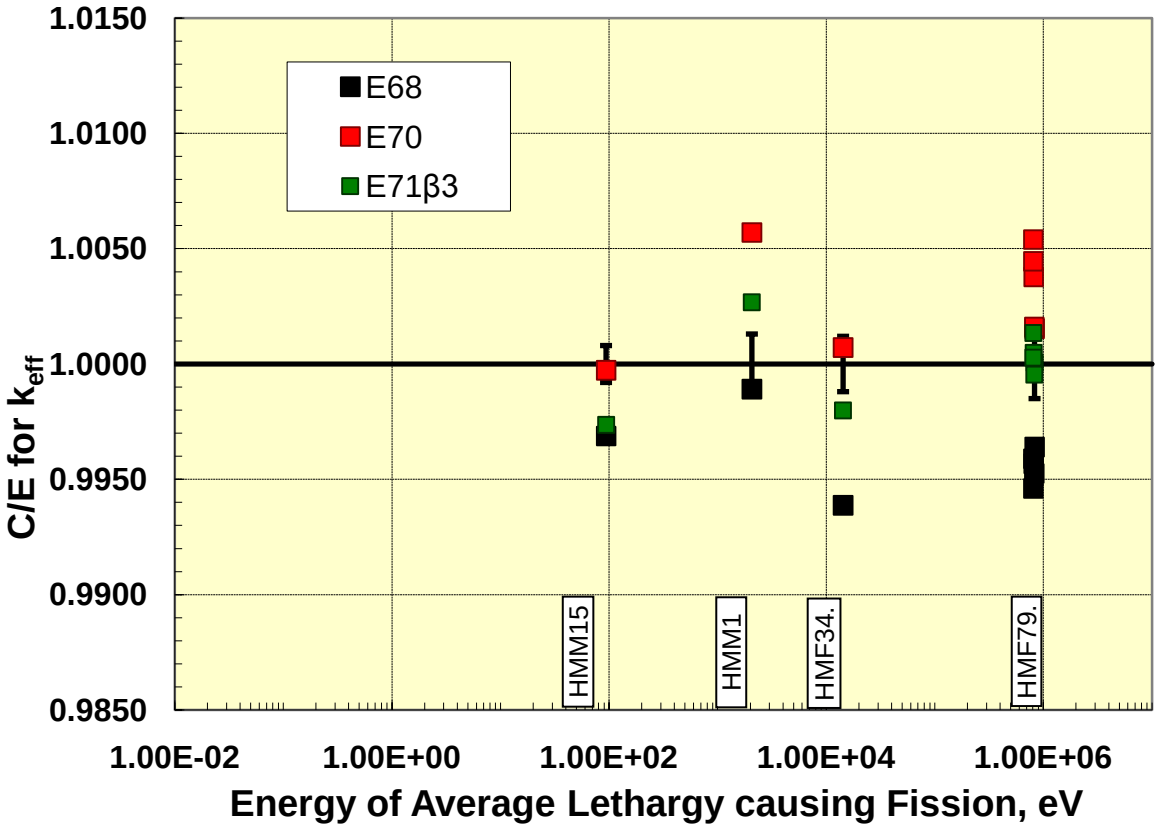

Fig. 3. Calculated eigenvalues for titanium bearing critical assemblies, shown as a function of average fission energy for that assembly. The near unity eigenvalues obtained support the conclusion that these new titanium cross sections are more accurate than those previously available and they do not exhibit an eigenvalue trend as a function of assembly energy.

The ENDF/B-VII.1 calculated eigenvalues are seen to fluctuate above and below unity versus energy, indicating no trend in calculated eigenvalue versus energy. Overall we conclude that the titanium isotopic cross section data in ENDF/B-VII.1 is superior to that available from earlier ENDF/B libraries.

Another structural material of importance whose cross sections have been revised for ENDF/B-VII.1 is tungsten. A suite of critical experiments using tungsten as an axial reflector of varying thickness or as a diluent were noted above (HMF49 and HMF50). In addition, diluent tungsten plus polyethylene has been used to test the cross section accuracy in the presence of a softer spectrum. Finally, critical systems using ^{239}Pu or ^{233}U have also been modeled. Calculated eigenvalues, with cross sections from ENDF/B-VI forward, are shown in Fig. 4.

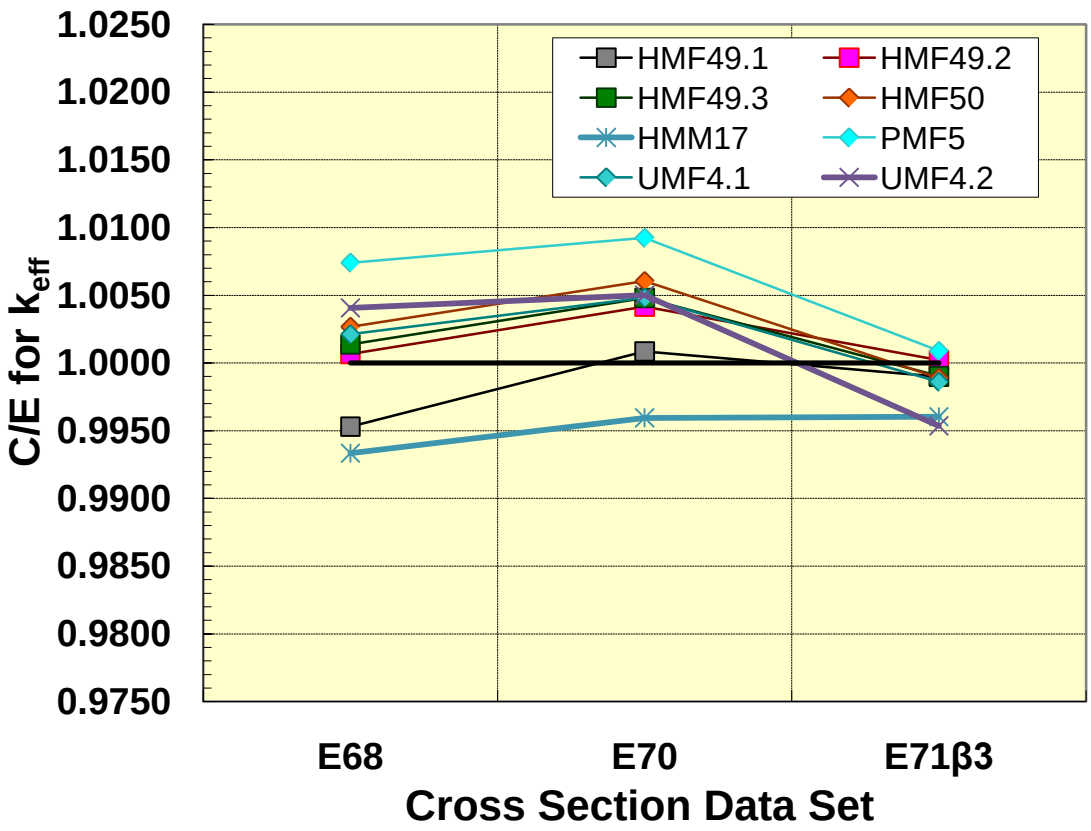

Fig. 4. Calculated eigenvalues for tungsten bearing critical assemblies. The reduced spread in calculated values with the latest cross sections compared to previous ENDF/B generations indicates a significant improvement in these latest evaluated files.

Going back to ENDF/B-VI, the average cross section was biased high by approximately 0.1%; a seemingly reasonable result. However, bare ENDF/B-VI HEU system eigenvalues were biased low by nearly 200 pcm, suggesting a bias of nearly 0.3% rather than 0.1% for tungsten bearing systems. ENDF/B-VII.0 failed to improve these calculated eigenvalues as average tungsten bearing system eigenvalue increased to a bias of nearly 0.4%. In addition, there was a large spread in calculated eigenvalues, varying by over 1% from a low of 0.996 to a high of 1.009. The revised tungsten cross sections appearing in ENDF/B-VII.1 are a significant improvement. The average calculated eigenvalue is now 0.9985; a marginally low but reasonable value in light of experimental uncertainties that are up to 160 pcm. Of greater import is the reduced spread in calculated eigenvalues, as the minimum to maximum variation now only spans an interval of 0.995 to 1.001.

Another material of interest and importance in reactor physics is beryllium. There are a large number of beryllium bearing benchmarks in the ICSBEP Handbook. Several of them represent systematic studies with a varying Be reflector thickness surrounding either HEU, ^{239}Pu or mixed HEU/Pu cores. These are geometrically simple systems, consisting of nested spheres. Some of their characteristics are summarized in Table 4.

Table 4. Characteristics for a selection of ICSBEP benchmarks that contain varying amounts of Beryllium. Multiple configurations for a given benchmark indicated that the combined arrangement of fuel and material differs, generally a decrease in the amount of fuel and an increase in reflector thickness. See the ICSBEP Handbook for details.

Bench-mark	Materials	Be Reflector Thickness, cm	Summary Description
HMF41, 2 cases	HEU/Be	4.6 11.8	External radial reflector
HMF58, 5 cases	Be/HEU/Be	0.5/ /20.3 0.5/ /9.3 0.5/ /5.4 0.5/ /3.3 0.5/ /2.2	Internal and external radial reflector

HMF66, 9 cases	Be/Be/HEU/Be	0.5/2.6//8.7 0.5/2.6//5.3 0.5/2.6//3.9 0.5/3.5//13.2 0.5/3.5//7.8 0.5/3.5//5.6 0.5/4.2//7.7 0.5/4.2//10.6 0.5/6.0//5.5	Two nested internal Be spheres + a variable HEU component + an external Be reflector
HMF77, 8 cases	Void/HEU/Be	9.3 5.7 14.7 8.6 6.3 8.8 4.5 6.9	Central void of varying radius + variable HEU component + an external Be reflector

MMF7, 23 cases	Pu/HEU/Be	20.0 – 1.36 17.3 – 0.67 10.2 – 1.23 3.57 – 0.66 2.66 – 1.50	Fixed Pu + increasing HEU + decreasing Be; repeat for 5 different Pu cores.

Unfortunately, the calculated eigenvalues from these benchmarks yield conflicting interpretations. Figs. 5 through 9 include calculated eigenvalues for ENDF/B-VI.8, ENDF/B-VII.0 and ENDF/B-VII.1 cross sections. Figs. 5, 6 and 7 display calculated eigenvalues for the HMF41, HMF58 and MMF7 benchmarks. These benchmarks had been most closely studied during the interim between ENDF/B-VI.8 and ENDF/B-VII.0. They generally exhibit a positive calculated eigenvalue bias with some evidence for an increasing bias with increasing reflector thickness when calculated with ENDF/B-VI.8 cross sections.

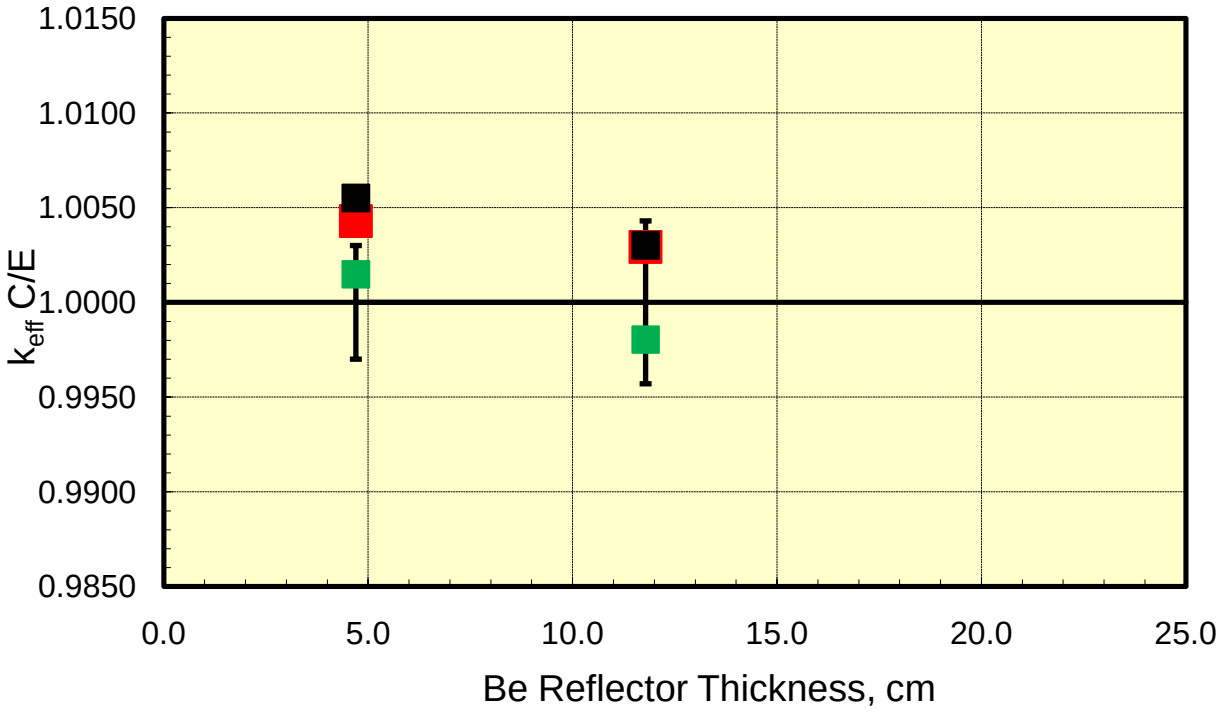

Fig. 5. Calculated eigenvalues with recent ENDF/B cross section libraries (red symbol is ENDF/B-VI.8; green symbol is ENDF/B-VII.0 and black symbol is ENDF/B-VII.1) for the HMF41 benchmark. Note that Figs. 5 through 9 use the same ordinate axis to portray to total range of beryllium reflector thicknesses over the entire benchmark suite.

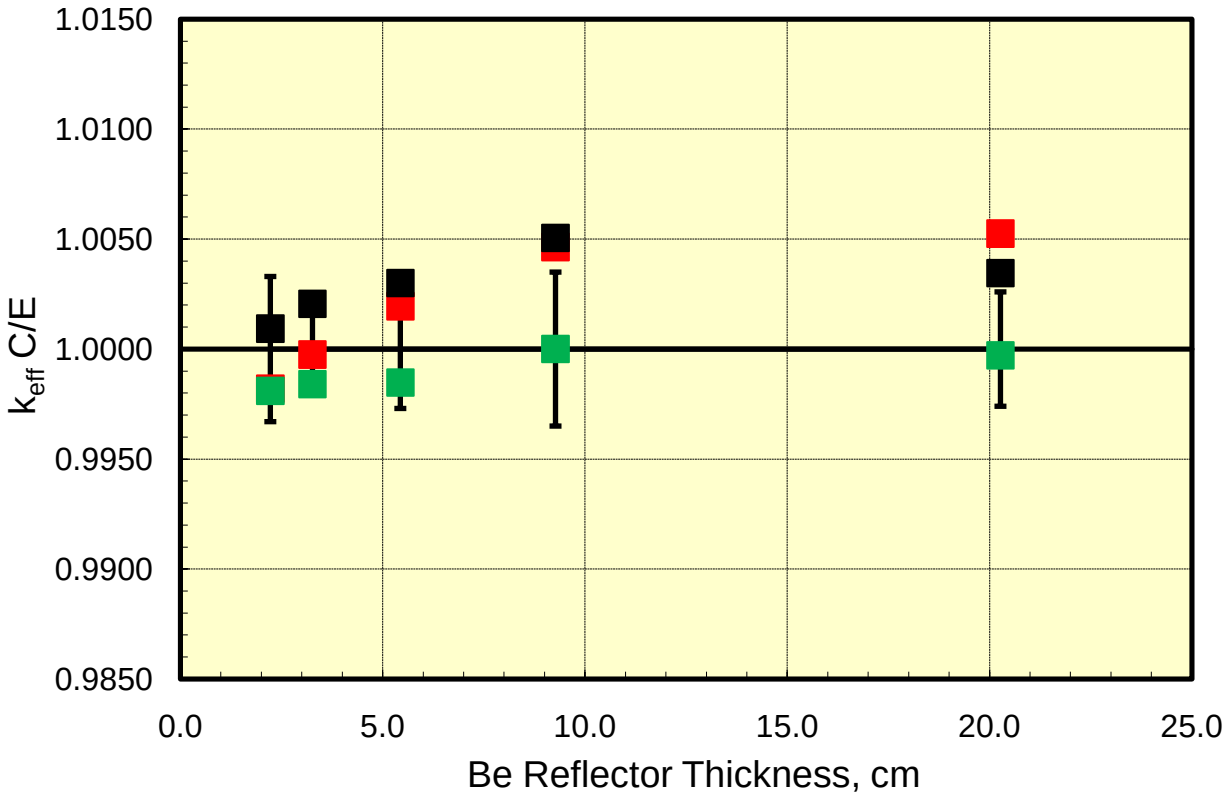

Fig. 6. Calculated eigenvalues with recent ENDF/B cross section libraries (red symbol is ENDF/B-VI.8; green symbol is ENDF/B-VII.0 and black symbol is ENDF/B-VII.1) for the HMF58 benchmark.

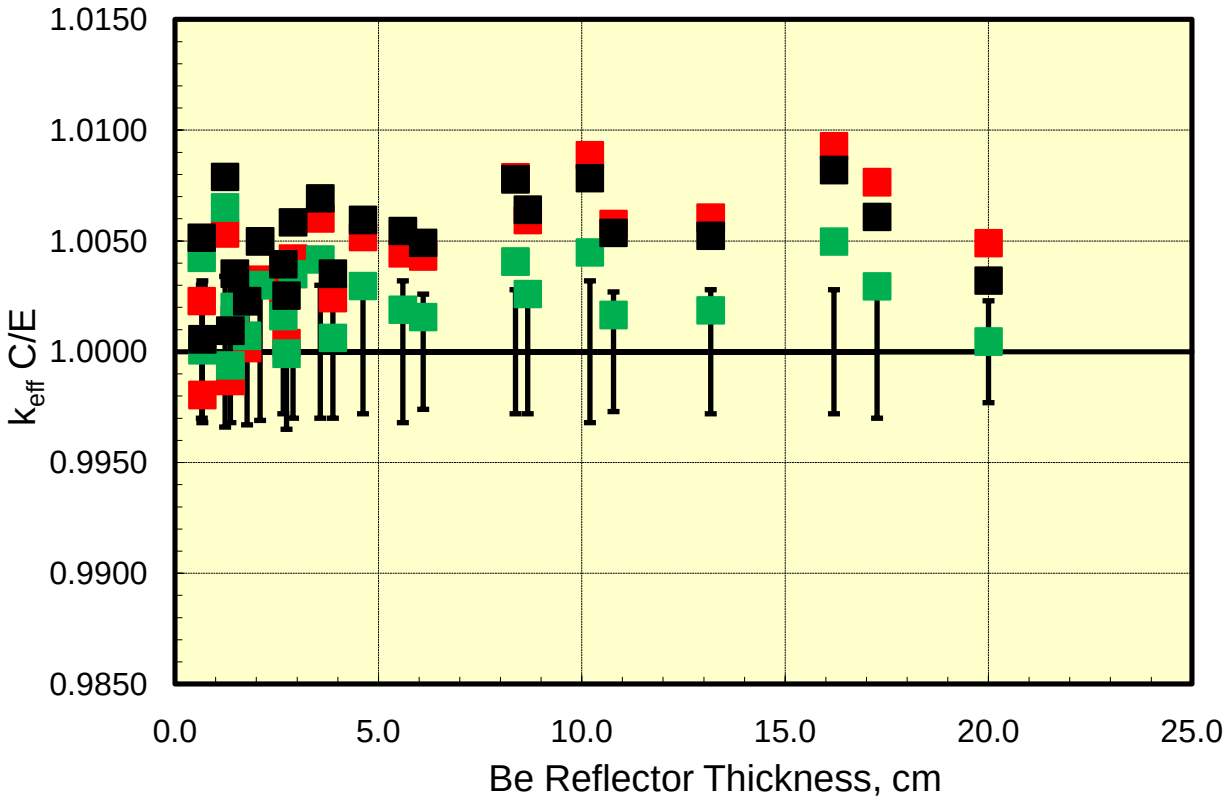

Fig. 7. Calculated eigenvalues with recent ENDF/B cross section libraries (red symbol is ENDF/B-VI.8; green symbol is ENDF/B-VII.0 and black symbol is ENDF/B-VII.1) for the MMF7 benchmark.

These observations lead to a re-evaluation of the Be cross sections for ENDF/B-VII.0 which tended to yield calculated eigenvalues significantly closer to unity with little or no evidence for a trend in calculated eigenvalue versus reflector thickness. Unfortunately, during the closing months prior to the release of ENDF/B-VII.0 new microscopic experimental data became available from RPI [6], and the HMF66 and HMF77 benchmarks were approved for publication in the ICSBEP Handbook. The new RPI data tended to be in better agreement with the ENDF/B-VI.8 Be evaluation, and the calculated

1

eigenvalues for HMF66 and HMF77 tended to be closer to unity with ENDF/B-VI.8 cross sections compared to ENDF/B-VII.0 (see Figs. 8 and 9), in direct contrast to the apparently more accurate calculated eigenvalues obtained with ENDF/B-VII.0 cross sections for the HMF41, HMF58 and MMF7 benchmarks. At that time it was decided to retain the revised ENDF/B-VII.0 Be evaluation, but it was clear that additional work on this cross section file was warranted.

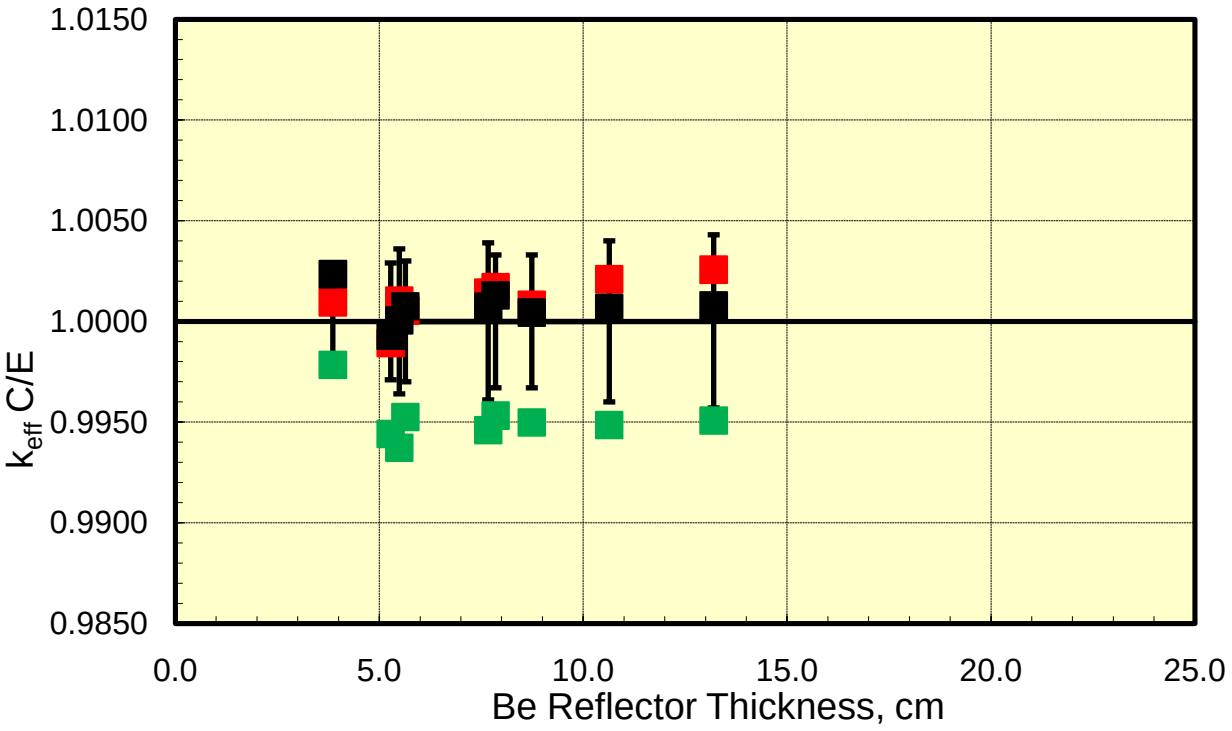

Fig. 8. Calculated eigenvalues with recent ENDF/B cross section libraries (red symbol is ENDF/B-VI.8; green symbol is ENDF/B-VII.0 and black symbol is ENDF/B-VII.1) for the HMF66 benchmark.

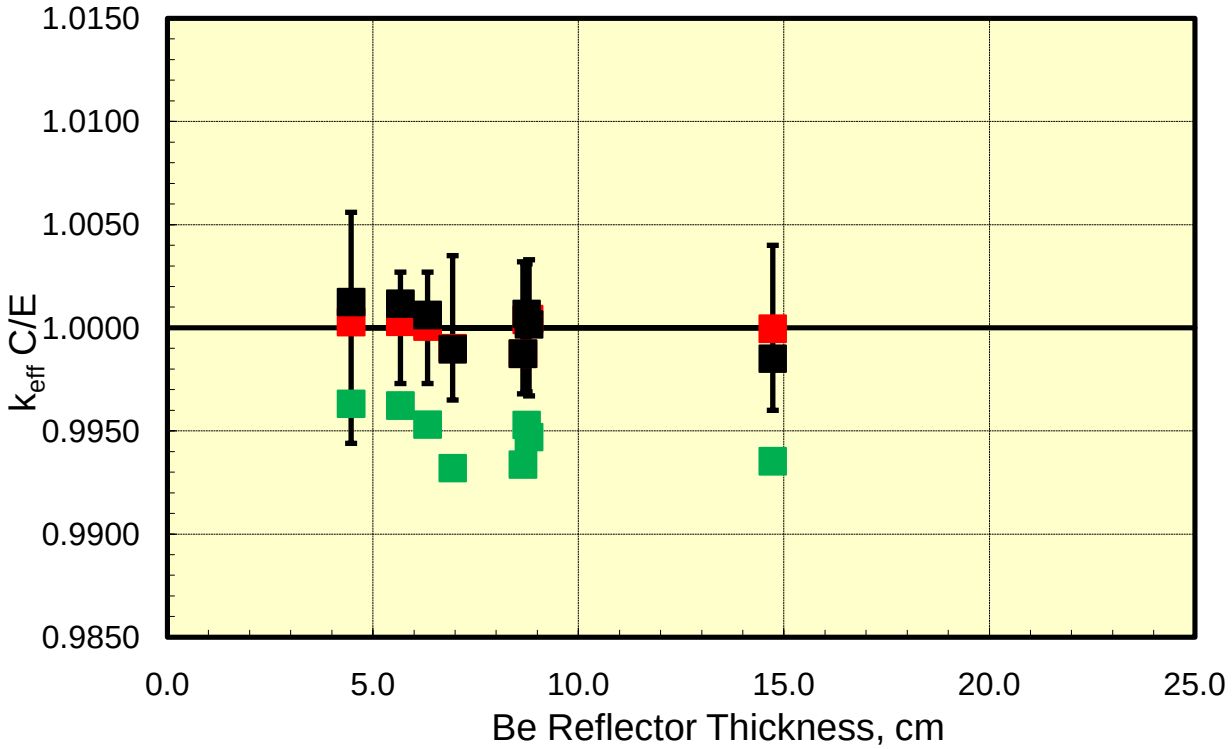

Fig. 9. Calculated eigenvalues with recent ENDF/B cross section libraries (red symbol is ENDF/B-VI.8; green symbol is ENDF/B-VII.0 and black symbol is ENDF/B-VII.1) for the HMF66 benchmark.

The revised Be evaluation that appears in ENDF/B-VII.1 includes the new RPI data and, not surprisingly, the cross sections and calculated eigenvalues are similar to those of ENDF/B-VI.8. However, the Be cross section file adopted for ENDF/B-VII.1 remains a work in progress. The basic cross section re-evaluation is believed to be complete, but a re-assessment of the scattering angular distributions has not been performed. This will be a future task, and if warranted such new distributions will be incorporated into a future ENDF release.

The HMF7 benchmark suite provides the opportunity to test cross section data over a broad energy range. This benchmark is only contains HEU and polyethylene. The HEU consists of 2.5 cm thick rectangular plates, either 25.4 cm x 25.4 cm or 12.7 cm x 25.4 cm in size. Various combinations of the HEU and similarly sized polyethylene plates are stacked into otherwise bare critical assemblies. A further softening of the spectrum is obtained by surrounding the 12.7 cm x 25.4 cm plates with a 12.7 cm thick external radial and axial polyethylene reflector. In summary, there are three broad classes of assemblies, (i) 25.4 cm x 25.4 cm HEU plates with or without interleaved polyethylene and no external reflector, (ii) 12.7 cm x 25.4 cm HEU plates with or without interleaved polyethylene and no external reflector and (iii) 12.7 cm x 25.4 cm HEU plates with or without interleaved polyethylene plus a 12.7 cm thick reflector on all sides. The ENDF/B-VII.1 calculated eigenvalues are illustrated in Fig. 10.

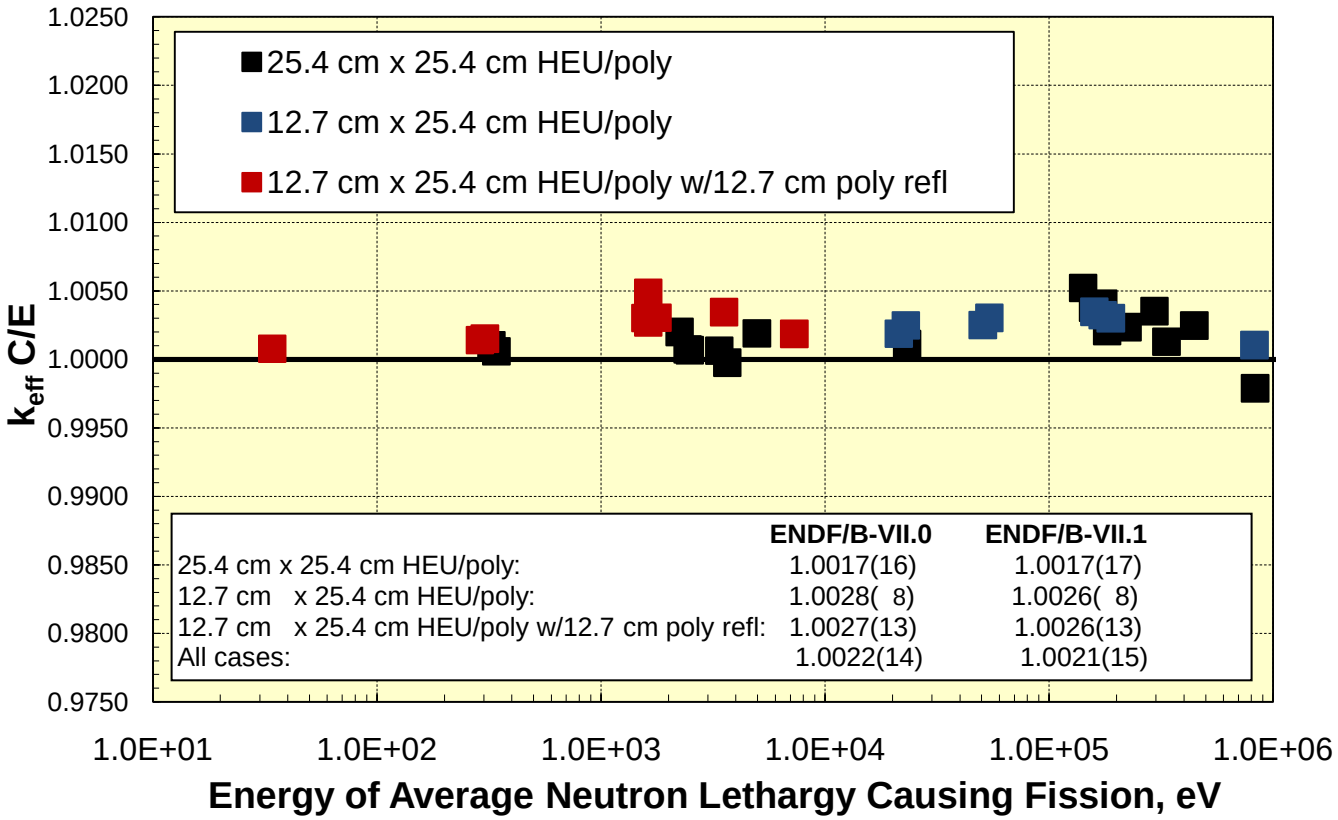

Fig. 10. ENDF/B-VII.1 Calculated eigenvalues for the HMF7 benchmark suite. The variable amount of polyethylene appearing in the many configurations of this suite allow for cross section data testing over a wide energy range.

This benchmark suite has been calculated previously with ENDF/B-VI.8 and ENDF/B-VII.0 cross sections. As the hydrogen, carbon and ^{235}U cross sections are little changed going from ENDF/B-VII.0 to ENDF/B-VII.1 there is correspondingly little change in the calculated eigenvalues. In general the calculated eigenvalues are within ~200 pcm of unity, with no statistically significant difference between the three configuration categories noted above. There is a possible small bias in calculated eigenvalues through the low to several hundred keV energy range but these data are not conclusive.

D. Thermal Systems

The ICSBEP Handbook contains many moderated assemblies suitable for cross section data testing. The simplest systems are solution assemblies in simple geometry; generally spheres or cylinders that contain little

more than the fissile material of interest, hydrogen and oxygen. Nitrogen or fluorine are also typically present but are often of limited neutronic importance. More complex systems include arrays of fuel rods, typically UO_2 fuelled. These arrays can be of various sizes, including groups of clusters or a single large rectangular or hexagonally oriented lattice. Reactivity control is maintained through various means, including cluster separation, water height, total number of fuel rods or presence of soluble poison. Most of the benchmarks reported below are water reflected, but we also provide limited results for lattice assemblies in the presence of lead, depleted uranium or steel (mostly iron) reflecting walls.

1. Solution Systems

The HEU-SOL-THERM (HST) benchmark class allows testing of thermal ^{235}U, hydrogen and oxygen data. Calculated eigenvalues are typically correlated against calculated Above Thermal Leakage Fraction, ATLF. This parameter varies significantly as a function of assembly geometry, and can serve as a qualitative measure of fission spectrum moderation. For geometrically large systems the fission neutrons are both born and moderated in the fissile solution, leading to a small ATLF value. For geometrically small systems the fission neutrons have a higher probability of escaping the solution, leading to a large ATLF. Until the early 1990s these benchmarks exhibited a significant bias in absolute k_{calc} and a large positive trend in k_{calc} with increasing ATLF. These issues were largely resolved due to Lubitz in ENDF/B-VI.3 and since then testing of this benchmark class is performed with the aim of verifying that the most recent upgrades to the underlying nuclear data retain the now accurate k_{calc} predictions.

Calculations with ENDF/B-VII.1 are shown in Fig. 11. Included are the results of a linear least squares fit of calculated eigenvalues correlated against ATLF. The regression analysis takes the form of $k_{predicted} = A_0 + B_0*ATLF$. Absence of a bias is signified when A_0 is found to be unity, or more specifically when its absolute value plus or minus its uncertainty encompasses unity. In the analyses reported here we report the 95% confidence interval (95CI) as the "uncertainty" used to assess whether the regression coefficient is statistically significant. The B_0 term is a measure of whether a trend in k_{calc} exists versus that regression parameter. Once again, the absolute value plus or minus the 95% confidence interval in that parameter prediction is used to conclude whether the postulated parameter trend is significant.

The HST benchmark suite contains 45 specific assemblies from ten HST benchmarks. These present experiments performed at either Oak Ridge National Laboratory or at Rocky Flats during the 1950s and 1960s. The assembly models are geometrically simple, consisting of spheres or cylinders and include unreflected and water reflected configurations. The resulting regression coefficients when using ENDF/B-VII.1 cross sections are $A_0 = 1.0000 \pm 0.0033$ and $B_0 = +0.0029 \pm 0.0088$. Since A_0 and its 95CI bracket unity and B_0 and its 95CI also bracket zero, we conclude that there is neither a bias nor trend versus ATLF in our reactivity calculations for this benchmark class. We note however that these regression parameters have changed compared to those obtained when fitting ENDF/B-VII.0 based k_{calc} values. Previously we determined $A_0 = 1.0007 \pm 0.0032$ and $B_0 = -0.0010 \pm 0.0085$. It can be dangerous to compare and judge whether two values that are within their respective uncertainties have changed, so we simply note that we have previously, and continue, to determine accurate near unity A_0 values, but the change in predicted B_0 is cause for concern. Expansion of this benchmark suite is warranted, in the hope that further experiments can be used to reduce the B_0 uncertainty. Alternatively, one might reassess the HST50 benchmark evaluation to see whether additional information can be extracted from the original log books to allow for a more consistent model with smaller modeling uncertainty. Currently the large variation in k_{calc} values among the 11 cases of this series of experiments are a significant contributor to the 95CI for this parameter that is simply too large.

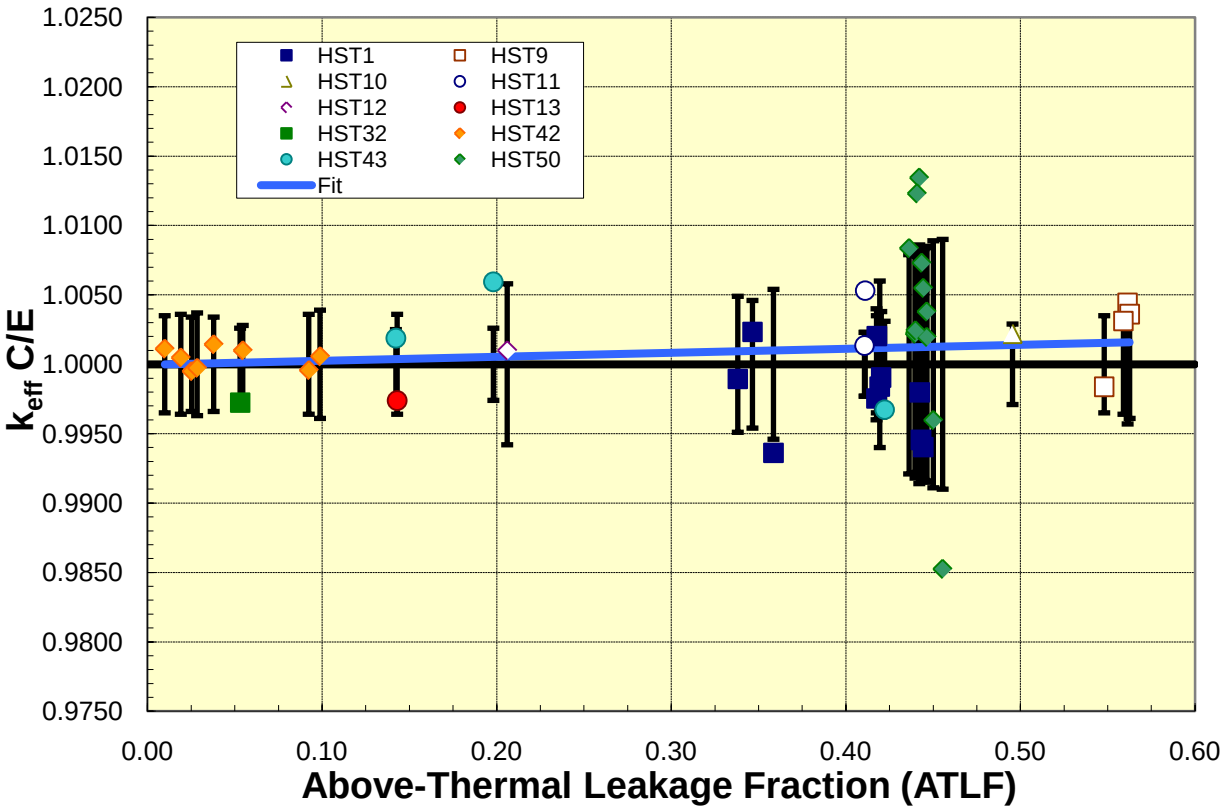

Fig. 11. Calculated eigenvalues for a suite of HEU-SOL-THERM benchmarks. This benchmark suite has been used for many years to validate thermal uranium critical assembly benchmark eigenvalue predictions. Results with ENDF/B-VII.1 cross sections are little changed from ENDF/B-VII.0, as expected, given that there has been minimal change in the underlying ^{235}U, hydrogen and oxygen evaluated cross section data.

A suite of more 150 PU-SOL-THERM benchmarks have been calculated in recent years with various cross section libraries. These benchmark models are geometrically simple and the only significant materials beside those needed to represent the thin-walled containers are plutonium, hydrogen, oxygen and nitrogen. Calculated eigenvalues for this class of benchmark have been biased high by approximately 0.5% in past ENDF/B libraries and this situation is unchanged for ENDF/B-VII.1 as the average k_{calc} for these benchmarks is 1.0055. The individual k_{calc} values vary from 0.9938 to 1.0188 and the population standard deviation is 0.0043. Corresponding values for ENDF/B-VII.0 were an average k_{calc} of 1.0047 and a population standard deviation of 0.0046.

Past analyses of HEU-SOL-THERM experiments have correlated k_{calc} versus Above-Thermal Leakage Fraction, ATLF. That correlation for the Pu-SOL-THERM experiments is shown in Fig. 12. Included in this figure are the predicted intercept and slope values and their associated 95CIs resulting from a linear least squares regression analysis. The calculated slope and its associated 95CI in k_{calc} versus ATLF is 0.0001 ± 0.0068. As we noted in the HST discussion, since the magnitude of the 95CI exceeds the magnitude of the slope we conclude that this slope value is statistically insignificant. This means there is no trend in calculated eigenvalue versus this parameter; a conclusion similar to that noted for the HST benchmark class. The other key regression coefficient is the intercept, 1.0055 ± 0.0024. In contrast to HST benchmarks, this intercept is significantly different from unity and is the basis for the ~0.5% k_{calc} bias noted in the opening paragraph of this section.

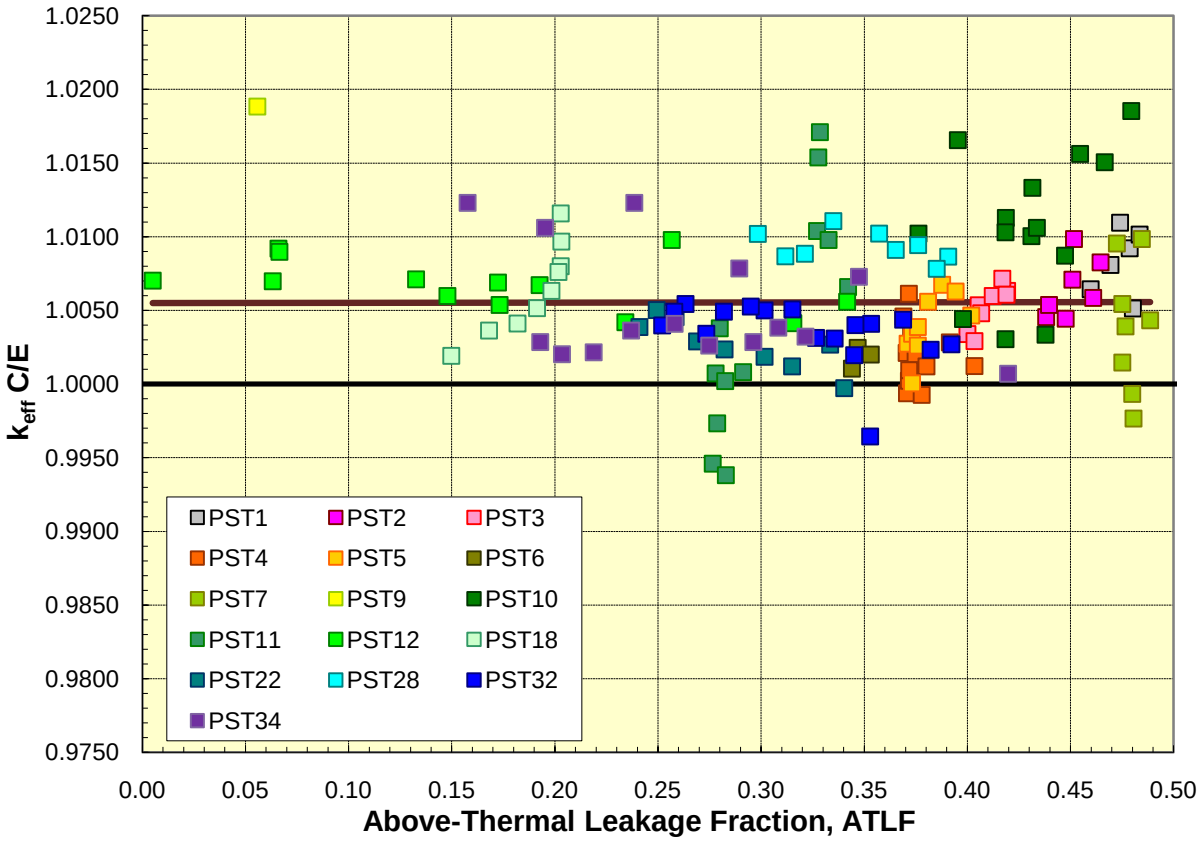

Fig. 12. Calculated eigenvalues for a suite of Pu-Sol-Therm benchmarks and the resulting correlation (solid brown line) with Above-Thermal Leakage Fraction, ATLF. Calculated regression coefficients are an intercept of 1.0055(24) and slope of 0.0001(68), where the values in parenthesis are 95% confidence intervals on the predicted coefficient. The slope is statistically insignificant but the intercept clearly deviates from unity by nearly 0.5%. This bias has been observed in past ENDF/B cross section libraries, and remains in ENDF/B-VII.1.

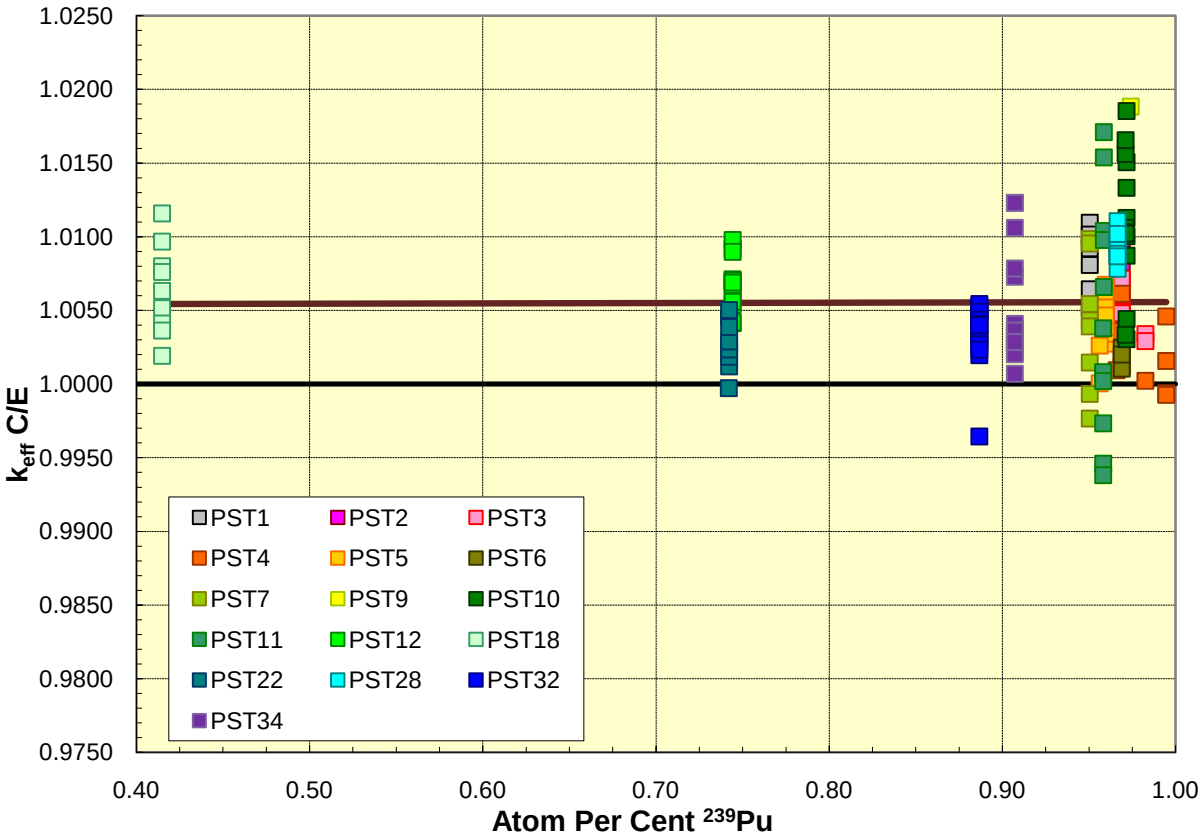

Fig. 13. Calculated eigenvalues for a suite of Pu-Sol-Therm benchmarks and the resulting correlation (solid brown line) with ^{239}Pu. Calculated regression coefficients are an intercept of 1.0053(44) and slope of 0.0003(49), where the values in parenthesis are 95% confidence intervals on the predicted coefficient. The slope is statistically insignificant but the intercept clearly deviates from unity by nearly 0.5%. This bias has been observed in past ENDF/B cross section libraries, and remains in ENDF/B-VII.1.

There are other parameters that could be considered for regression analysis in the hope that a statistically significant trend is observed that could be related to some aspect of the underlying nuclear data. Among these are the ^{239}Pu atom fraction, which varies from a low of ~0.4 to > 0.99. k_{calc} values are plotted against this parameter in Fig. 13 and the linear regression parameters for this and several other potential parameters are provided in Table 5. Once again no trend is observed, as the ^{239}Pu atom fraction slope parameter is determined to be 0.0003 ± 0.0049. As then expected, the intercept term is virtually unchanged from that obtained in the ATLF regression, 1.0053 ± 0.0044. Note however even the absence of a trend in the face of a constant bias provides important information. In this instance, lack of a trend in k_{calc} suggests that the underlying bias is not due to a unique aspect of ^{239}Pu nuclear data since the observed bias remains constant as the ^{239}Pu content varies.

Other parameters that have been studied include Above Thermal Fission Fraction, ATFF; g Pu per liter; different measures of the average fission energy; or various calculated reaction fractions including ^{239}Pu capture or fission and hydrogen capture. Regression coefficients for these parameters are summarized in Table 5.

It is apparent from Table 5 that all predicted slope coefficients are statistically insignificant. Hence there is no single experimental parameter that easily accounts for the k_{calc} bias. Alternatively, lack of a trend in k_{calc}, supports the argument that the underlying nuclear data behind that parameter are likely not the cause of this bias. Specifically lack of a trend in k_{calc} when correlated with calculated ^{239}Pu capture, ^{239}Pu fission and hydrogen capture all indicate that these data are reasonably accurate. Also, lack of a trend in k_{calc} versus a basic benchmark model parameter such as g Pu per liter or H/Pu number density ratio suggests that these fundamental solution characteristics are properly defined.

Table 5. Calculated regression coefficients for a suite of PST benchmark assemblies, correlated against various critical assembly parameters. Although there is a clear bias in the average calculated eigenvalue for this

benchmark class, there is no evidence for a trend in calculated eigenvalue versus any tested parameter.

Parameter	Intercept & 95% CI *	Slope & 95% CI *
Above Thermal Leakage Fraction, ATLF	1.0055(24)	+0.0001(68)
Above Thermal Fission Fraction, ATFF	1.0057(9)	-0.0028(89)
^{239}Pu/Pu atom fraction	1.0053(44)	+0.0003(49)
g Pu/liter	1.0056(9)	-1.31(8.39)e-6
Energy of Average Lethargy causing Fission, eV	1.0058(8)	-0.0012(16)
Average Fission Energy, eV	1.0057(9)	-1.21(3.25)e-8
^{239}Pu Production Fraction	1.0062(109)	-0.0007(112)
^{239}Pu/Pu Capture Fraction	1.0049(34)	+0.0008(42)
Hydrogen (in solution) Capture	1.0057(12)	-0.0020(112)
H/Pu Number Density Ratio	1.0057(12)	-0.32(1.66)e-6
* Values in parenthesis represent the 95CI in the corresponding least significant digits.		

It is a simple fact that an eigenvalue bias exists for the PST benchmark class. This bias has been present through all generations of ENDF/B libraries, and it remains so with these latest data.

2. Low Enriched Lattice Systems

LEU-COMP-THERM (LCT) is an important benchmark class, as these benchmarks span the range of nuclear parameters, particularly uranium enrichment, moderation and soluble or lumped poisons that are important to the commercial reactor industry. The ICSBEP Handbook contains nearly 100 LCT evaluations. Those that have been calculated with the new ENDF/B-VII.1 library are summarized in Table 6.

Table 6. Selected attributes for a suite of LEU-COMP-THERM benchmarks. Further details are available from the ICSBEP Handbook.

Benchmark	Fuel	Comment
LCT1 (8 cases)	$U(2.35)O_2$	Water moderated and reflected.
LCT2 (5 cases)	$U(4.31)O_2$	Water moderated and reflected.
LCT6 (18 cases)	$U(2.6)O_2$	Water moderated and reflected.
LCT7 (10 cases)	$U(4.738)O_2$	Water moderated and reflected.
LCT8 (6 cases)	$U(2.459)O_2$	Borated water moderated and reflected; also may include water holes and poison rods.
LCT10 (13 cases)	$U(4.31)O_2$	Water moderated with Lead, Uranium or Steel plus water reflectors. Same fuel as LCT2.
LCT11 (5 cases)	$U(2.5)O_2$	Borated water moderated and reflected. Fuel lattice includes water holes.
LCT17 (14 cases)	$U(2.35)O_2$	Water moderated with Lead, Uranium or Steel plus water reflectors. Same fuel as LCT1.
LCT22 (7 cases)	$U(10.0)O_2$	Water moderated and reflected
LCT024 (2 cases)	$U(10.0)O_2$	Water moderated and reflected
LCT25 (4 cases)	$U(7.5)O_2$	Water moderated and reflected
LCT27 (4 cases)	$U(4.738)O_2$	Water moderated with Lead plus water reflectors. Same fuel as LCT7.
LCT35 (3 cases)	$U(2.6)O_2$	Water moderated and reflected, includes either soluble boron or gadolinium. Same fuel as LCT6.
LCT39 (10 cases)	$U(4.738)O_2$	Water moderated and reflected. Same fuel as LCT7, now include water holes.

Resolution of the longstanding negative calculated eigenvalue bias for UO_2 fuel systems was an ENDF/B-VII.0 success story. With essentially no change in the uranium or oxygen cross sections for ENDF/B-VII.1 we expect to retain this good calculated eigenvalue performance. Fig. 14 displays the calculated eigenvalues for a selection of the ICSBEP LEU benchmarks. These systems encompass experiments from throughout the world, including the United States, France, Russia and Japan. It is clear from the figure that accurate eigenvalue calculations for this class of benchmark are obtained with ENDF/B-VII.1 cross sections.

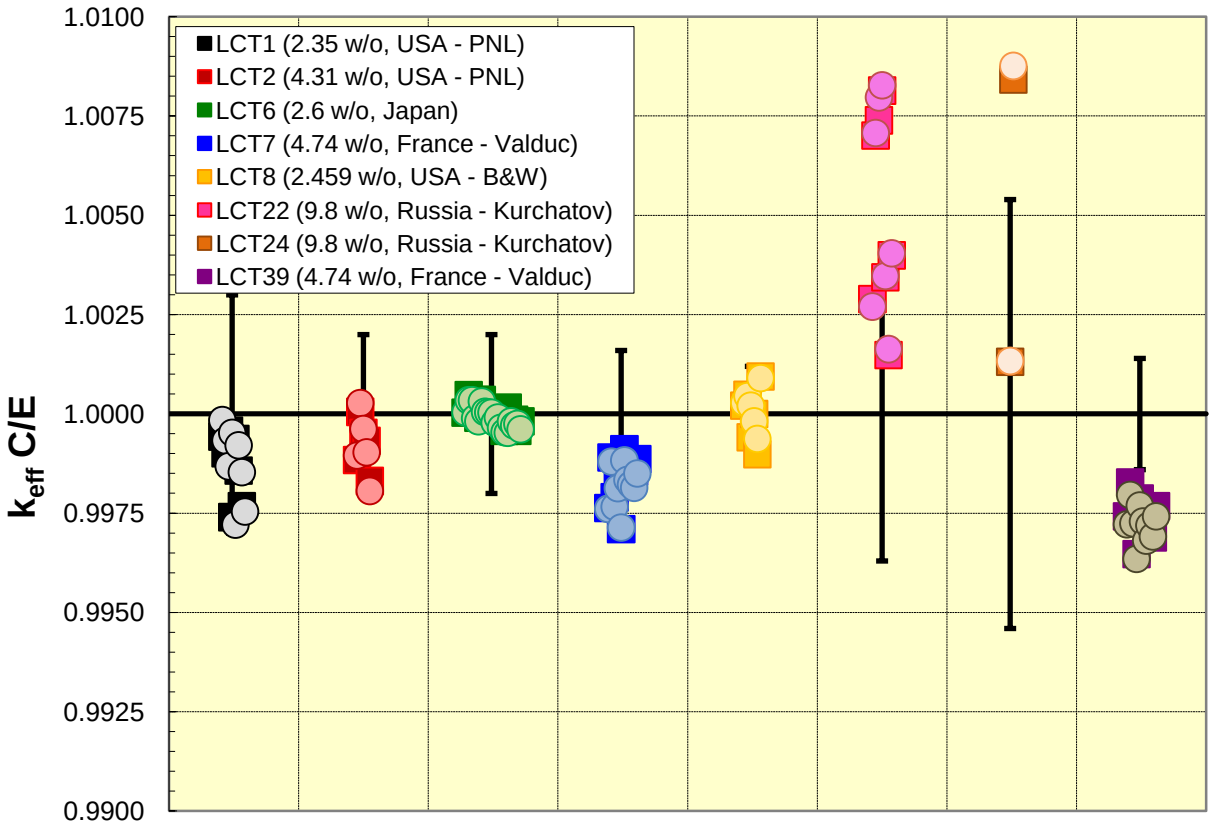

Fig. 14. Calculated eigenvalues (solid squares are ENDF/B-VII.0, lighter circles are ENDF/B-VII.1) for a suite of LEU-COMP-THERM benchmarks. ENDF/B-VII.1 results are virtually identical to ENDF/B-VII.0, as expected, and are generally within the experimental uncertainty.

These experiments are all water moderated, but span a range of enrichments (from ~2.3 w/o to ~10 w/o), and span a range of moderations. They are all thermal systems, but the combination of fuel diameter, rod diameter and lattice pitch yield all combinations of undermoderated, near optimally moderated and overmoderated systems. These benchmarks range in size from small arrays of clusters containing as few as a hundred rods each to large single clusters with more than 1000 rods. Regardless of the degree of moderation, accurate eigenvalue calculations are obtained, as the majority of the calculated eigenvalues are within the one sigma experimental uncertainty and it is apparent that all are within the two sigma uncertainty.

Calculations of the LCT10 and LCT17 benchmarks are another example where a previous benchmark from the ICSBEP Handbook serves as a base case. LCT10 utilizes the same fuel rods as were present in the water moderated LCT2 benchmark, but now includes large reflecting walls of either Lead, depleted Uranium or Steel (mostly Iron) aligned along two sides of these clusters. Similarly LCT17 uses these same reflecting materials plus LCT1 fuel. Multiple configurations where the reflector walls are positioned immediately adjacent to the lattice, then moved perpendicularly away from the fuel, thereby allowing for varying amounts of water between the fuel and reflector are defined. k_{calc} C/E results for ENDF/B-VII.0 and ENDF/B-VII.1 calculations are illustrated in Fig. 15.

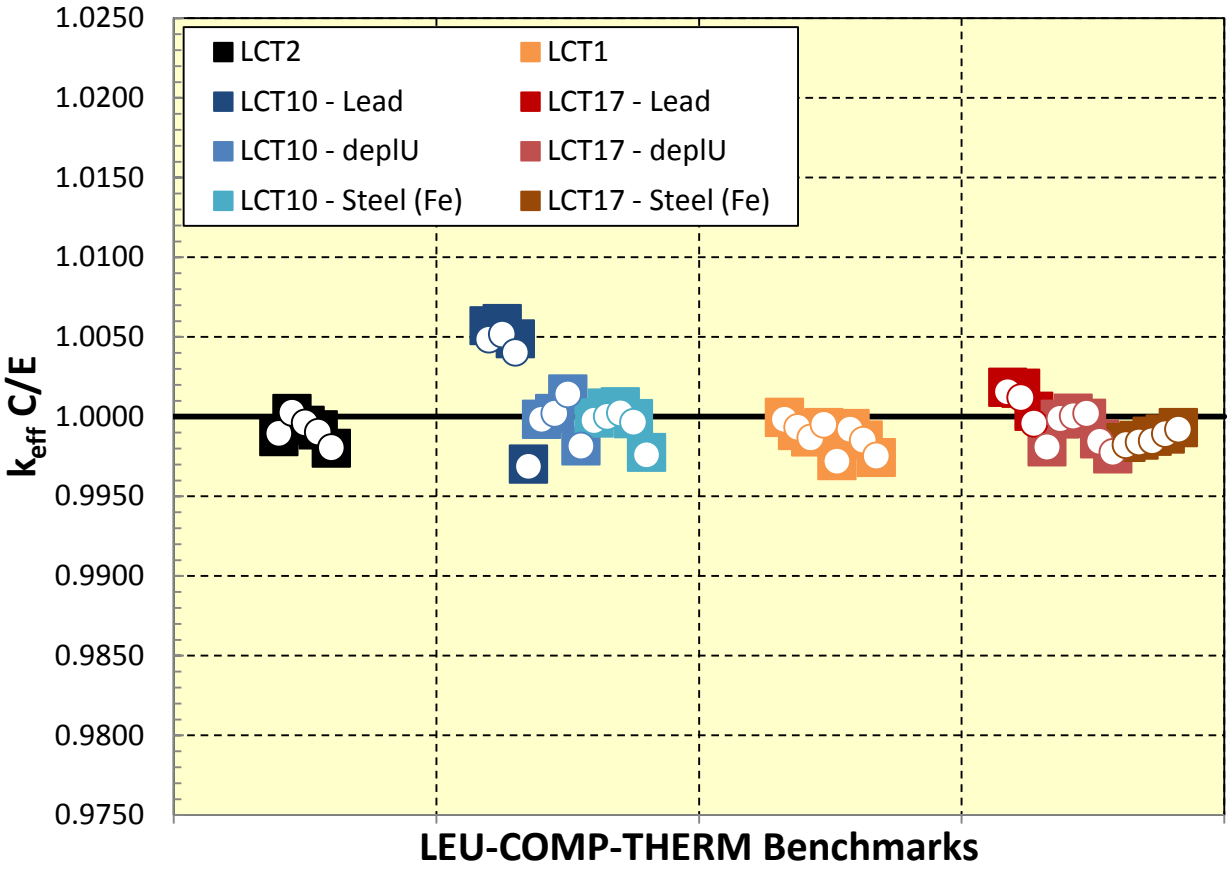

Fig. 15. Calculated eigenvalues (solid square are ENDF/B-VII.0, open circles are ENDF/B-VII.1) for LEU-COMP-THERM benchmarks with water only or water plus one of lead, depleted uranium or steel (iron) reflectors. LCT2 and LCT10 contain the same fuel and cluster/lattice geometry, with LCT2 serving as a water reflector only base case. Metallic reflector walls were place in multiple locations, leading to 3 or more critical assembly configurations for each material. See the ICSBEP Handbook for additional details.

There are four sets of calculated eigenvalues portrayed here. The leftmost set, LCT2, serves as a base case for the LCT results that appear next. Both LCT2 and LCT10 use the same fuel, arranged in virtually identical configurations. The lattice pitch is 2.54 cm for both and the cluster arrangement is a triplet of 13 x 8 clusters arranged the 13 rod row. The reflecting walls are positioned parallel to the 13 rod row and vary in location from immediately against the lattice or pulled away by up to 5.4 cm. The rods and walls are immersed in water and cluster separation, varying from ~20 cm to less than 10 cm is used to attain criticality. For LCT10 there are four discrete measurements with Lead and ^{depl}U walls and five measurements with steel. All but three of the calculated LCT10 eigenvalues are tightly clustered and in good agreement with the LCT values. Three configurations, for lead walls immediately adjacent to the clusters, or pulled back by either 0.66 cm or 1.32 cm yield high calculated eigenvalues. For the fourth Lead configuration the wall to lattice separation is ~5.4 cm, a distance large enough that reflection has little impact upon the calculated eigenvalue. The next two sets of calculations in Fig. 15 are for the LCT1 (base case) and LCT17 benchmarks. Once again the base geometry is a set of three clusters, now 19 x 16 rods set on a 2.03 cm pitch, with the reflecting wall located immediately adjacent the assembly and then moved perpendicularly away. Three measurements were made with a Lead wall, six measurements with ^{depl}U and five with steel. All reflected configuration calculated eigenvalues are in reasonable agreement with the base case, although close examination of these calculated eigenvalues still reveals a bias for the Lead reflector case. This bias is much smaller; likely a consequence of a larger lattice compared to LCT10 and so the production coming from interior lattice rods that are farther away from the wall is not affected. In contrast, the French LCT27 experiment places thin Lead walls on all four sides of a 14 x 14 rectangular lattice. The lead walls are immediately adjacent to the lattice, and then successively moved back 0.5 cm to a maximum of 1.5 cm from the lattice. Once

again a large calculated eigenvalue bias is observed, averaging over 800 pcm. Lead cross sections are unchanged in ENDF/B-VII.1 compared to ENDF/B-VII.0, but it seems clear that there are deficiencies in these evaluations that lead to an overprediction of calculated eigenvalues. While an overprediction may be viewed by some in the criticality safety community as better than an underprediction, the opposite conclusion would be drawn by the shielding community since a consequence of calculating too much reflection back into the assembly means that a prediction of shield effectiveness would likely underpredict the number of neutrons (and therefore the dose) due to neutrons the penetrate that shield. Clearly further evaluation work on the Lead cross sections is needed.

E. ^{233}U Systems

^{233}U is little changed from that in ENDF/B-VII.0, and in fact the majority of data testing performed during the beta evaluation phase of ENDF/B-VII.1 used the ^{233}U ENDF/B-VII.0 file. At a recent International Atomic Energy Agency (IAEA) Consultant's meeting on the adequacy of ^{233}U cross section data for the ^{233}U/Th fuel cycle it was noted that the low energy inelastic scattering cross section displayed a seemingly unphysical bump; an artifact of the earlier ENDF/B-VI based evaluation that had been carried forward into ENDF/B-VII.0. Recent calculations, described in [2] have reduced this feature and represents the only cross section change to the evaluated ^{233}U file in going from ENDF/B-VII.0 to ENDF/B-VII.1.

^{233}U bearing benchmarks from the ICSBEP Handbook that have been calculated include ten FAST systems. Among these are a bare sphere, U233-MET-FAST-001, or UMF1, a ^{nat}U reflected sphere, UMF6, as well as ^{233}U spheres reflected by varying amounts of uranium, tungsten or beryllium. Calculated eigenvalues for ENDF/B-VII.0 and ENDF/B-VII.1 are shown in Table 7.

Table 7. Calculated eigenvalues for a suite of ICSBEP Handbook U233-MET-FAST benchmarks.

Benchmark	ENDF/B-VII.0 k_{eff} C/E *	ENDF/B-VII.1 k_{eff} C/E *	Comment
UMF1	0.99964(4)	0.99994(8)	bare
UMF2	0.99907(4) 1.00050(4)	0.99882(8) 1.00053(8)	HEU reflector
UMF3	0.99945(4) 1.00016(4)	0.99945(9) 1.00009(9)	^{nat}U reflector
UMF4	1.00459(4) 1.00500(4)	0.99893(9) 0.99591(9)	W reflector
UMF5	0.99427(4) 0.99248(4)	0.99630(9) 0.99599(9)	Be reflector
UMF6	0.99928(4)	0.99898(10)	LANL Flattop-23

* Values in parenthesis represent the uncertainty in the corresponding least significant digits.

As with all data testing results reported throughout this paper there are two questions to answer. First, are those benchmarks that are accurately calculated with ENDF/B-VII.0 cross sections still accurately calculated with the latest cross sections, and secondly, are those benchmarks that exhibited significant ENDF/B-VII.0 based k_{calc} deviations from unity now calculated more accurately?

From Table 7 we note that those UMF benchmarks whose reactivity was accurately calculated with ENDF/B-VII.0 continue to be accurately calculated, as the near unity k_{calc} values for UMF1, UMF2, UMF3 and UMF6 are retained. As noted previously, a significant revision to the W cross sections has occurred and we continue to see their impact upon calculated reactivity, with the previous ~500 pcm overprediction now being a ~100 to ~400 pcm underprediction. Also, the Be reflected systems exhibit a reactivity increase consistent with that observed for other (HEU, Pu and MIX) FAST systems. In general the average k_{calc} value is improved. For the benchmark configurations tabulated above the average k_{calc} and the standard deviation of the ten sample population for ENDF/B-VII.0 and ENDF/B-VII.1 are 0.9989(42) and 0.9985(18), respectively. Although the average eigenvalue for ENDF/B-VII.1 has decreased compared to ENDF/B-VII.0, the more important change is in the population standard deviation which has decreased significantly, from 0.0042 to 0.0018. This is due to the large decrease in calculated eigenvalue for the previously overpredicted W reflected systems and the modest increase in calculated eigenvalues for the previously underpredicted Be reflected systems. k_{calc} for bare and uranium reflected systems were accurately calculated with ENDF/B-VII.0 cross sections and they remain so with ENDF/B-VII.1 cross sections.

There are a large suite of U233-SOL experiments in the Handbook that span the INTER and THERM categories. These include unreflected systems as well as one or more of water, polyethylene and beryllium reflectors. As shown in Fig. 16, there is a significant trend in k_{calc} when plotted versus energy. This is a characteristic of ENDF/B-VII.0 and earlier cross sections, and remains so with the most recent cross sections. The only difference of note with the ENDF/B-VII.1 cross sections compared to ENDF/B-VII.0 is a small but uniform increase in calculated reactivity, similar to that seen in other SOL experiments. As noted previously this is due to the small increase in ^{16}O's elastic scattering cross section.

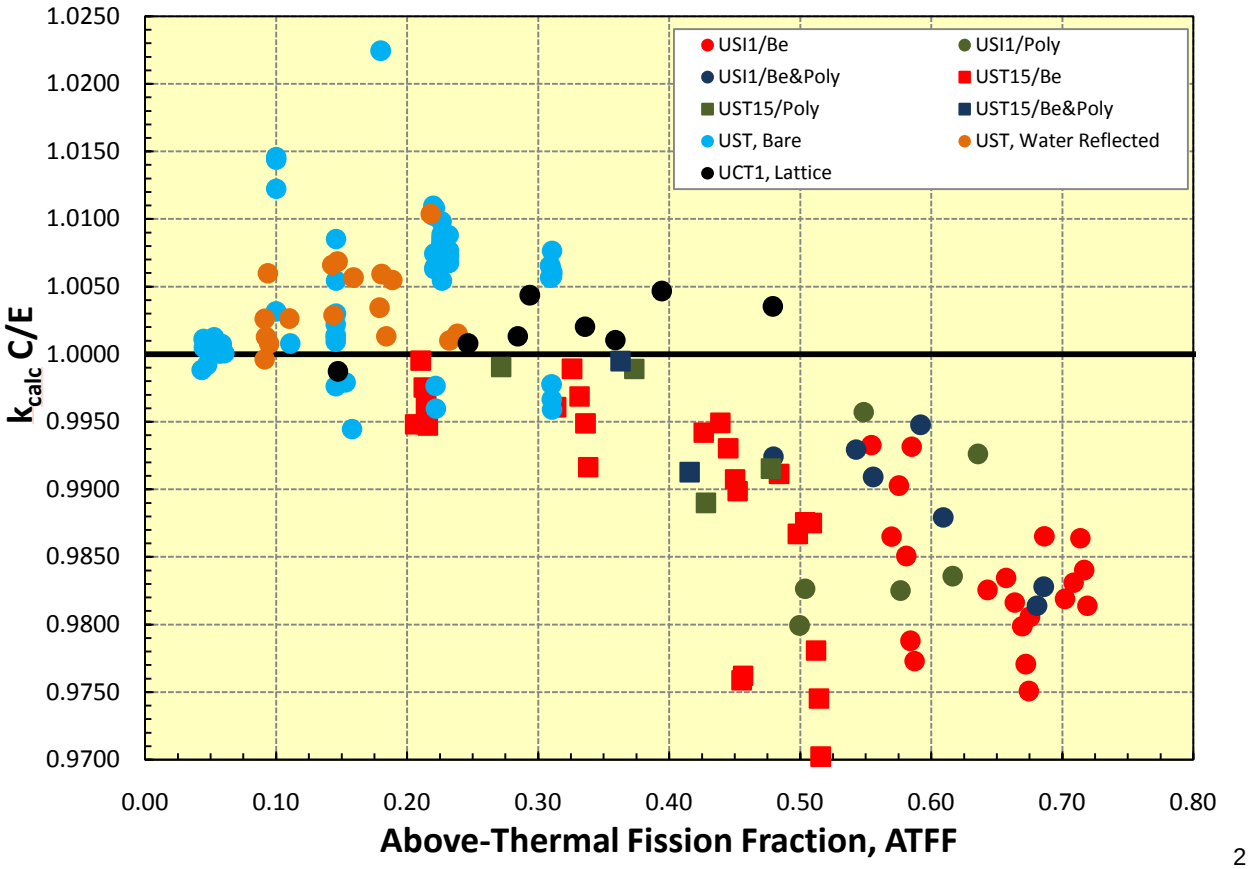

Fig. 16. Calculated eigenvalues for a suite of U233-SOL-THERM and U233-COMP-THERM benchmarks. Moderating materials include one or more of water, polyethylene and beryllium. Accurate eigenvalue predictions are obtained for the most thermal systems, and a bias of less than 0.5% is observed for the Light Water Breeder Reactor Seed-Blanket (UCT1) benchmarks, but otherwise there is a clear trend in calculated eigenvalue versus Above-Thermal Fission Fraction.

Also shown on Fig. 16 are k_{calc} values for UCT1. This experiment is a lattice of fuel rods containing various combinations of $^{233}UO_2$, $^{235}UO_2$ and ThO_2. Collectively these experiments are sometimes referred to as the "LWBR SB" experiments, for "Light Water Breeder Reactor, Seed-Blanket". These critical experiments were performed as part of the United States' LWBR program in the 1960s and 1970s. The k_{calc} values for these experiments generally fall within the trend established by the U233-SOL experiments and occur at an average Above-Thermal Fission Fraction value that fortuitously is near unity. We conclude this discussion noting that the most highly thermalized systems, characterized by ATFF values near 0.05 are accurately calculated and, as summarized in Table 7 above a number of FAST systems (whose ATFF values are unity) are also accurately calculated. This suggests that the thermal and high energy (hundreds of keV and higher) cross sections for ^{233}U are likely accurate. It is deficiencies in ^{233}U nuclear data over a broad range of intermediate energies that are likely responsible for the observed k_{calc} trend.

F. Argonne ZPR Systems

Detailed as-built models are available for a series of Argonne ZPR/ZPPR critical assemblies. These models represent the physical dimensions and masses of each and every plate, can, drawer and matrix tube and the interstitial gaps among these materials for the as-built material loadings for each of these assemblies. It is now practical to produce high-fidelity models of these assemblies and to calculate these experiments using continuous-energy Monte Carlo methods. Simplified models of most of these experiments are also available in the ICSBEP Handbook and, results of performance testing with ENDF/B-VII.1 data for these many of these models are also reported in Appendix B of this paper. It should be noted that, because only very small corrections or biases are required with the use of the detailed models of these experiments to account for simplifications of the model, the associated uncertainties (and potential biases) in these models are smaller than those for the simplified benchmark models.

To test the performance of the new ENDF/B-VII.1 evaluations, analyses of these detailed models were performed by Argonne using MCNP5 and NJOY with both ENDF/B-VII.0 and -VII.1 data. Four types of experiments (criticality, β_{eff}, sodium-void worth and control rod worth) are analyzed.

1. Criticality Measurements

Measurements of criticality (and/or sub-criticality) for 38 Argonne ZPR/ZPPR configurations, including 13 high enriched uranium (HEU) configurations, nine intermediate enriched uranium (IEU) configurations, 14 mixed-(Pu, U) configurations, and two Pu metal configurations have been analyzed. The performance of the new ENDF/B-VII.1 library versus the performance of the ENDF/B-VII.0 are displayed for these four groups – HEU, IEU, mixed-(Pu, U) and Pu-metal – in Figs. 17 – 20, respectively. In all of these figures the y-axis, or ordinate, represents (C/E – 1) x 10^5, i.e., the fractional deviation between the calculated k_{eff} and the experimental k_{eff}, in pcm. The ICSBEP identifier for the critical assembly is displayed on the abscissa. The standard ZPR/ZPPR assembly numbers are displayed as "labels" with each of the data values. The order of the assemblies, with the exception of the three mixed-(Pu, U) assemblies which are not provided in the ICSBEP Handbook, is always from hardest neutron spectrum (left side) to softest spectrum (right side), as determined by the values of EALF and the fraction of fissions at energies > 100 keV as given in the neutron balance tables in the Handbook.

The results obtained for the HEU-fueled assemblies (see Fig. 17) indicate that all 13 assemblies were over-predicted with ENDF/B-VII.0 data. The average ENDF/B-VII.0 k_{eff} bias is in excess of 1% δk/k (1042 pcm); the largest bias (ZPR-9/4) was almost 2% δk/k (1948 pcm). All 13 k_{eff}'s are reduced with ENDF/B-VII.1 cross sections and the average k_{eff} bias is now <0.5% δk/k (463 pcm). Notably, the bias for ZPR-9/4 was reduced by >1.2% δk/k to ~0.7% δk/k with ENDF/B-VII.1 data. Only the bias for the ZPPR-20E assembly, an accident scenario for a space application with an HEU core containing lithium and reflected with beryllium oxide and silicon dioxide, was not significantly reduced (from +1685 ± 800 pcm to +1490 ± 800 pcm). The ZPPR-20E experiment was very subcritical and had the largest experimental uncertainty among the full set of 38 configurations. The last of the experiments displayed in Fig. 16 is for ZPR-9/34, a Uranium/Iron assembly. This is a clean physics benchmark assembly with an intermediate spectrum, having only ~40% of the fissions occurring above 100 keV. The over-prediction of k_{eff} for this assembly, almost 1% δk/k (882 pcm) with ENDF/B-VII.0, is reduced to +217 ± 111 pcm with ENDF/B-VII.1.

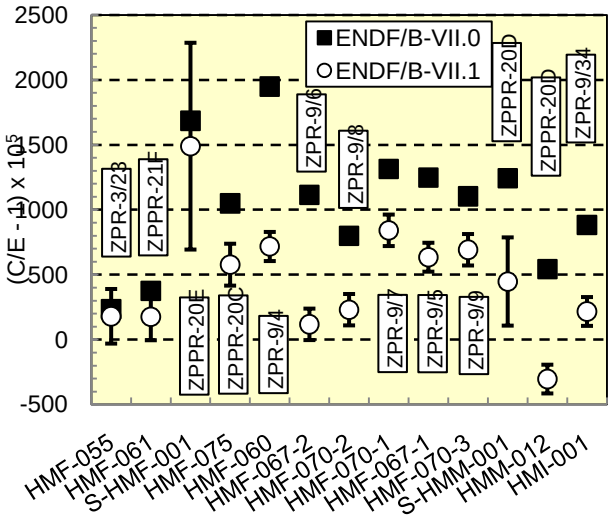

Fig. 17. MCNP calculations with "As-Built" models for HEU FAST and INTER ZPR/ZPPR Assemblies.

The k_{eff} results obtained for the IEU-fueled assemblies (see Fig. 18) indicate that seven of the nine assemblies are over-predicted with ENDF/B-VII.0 cross sections. The average ENDF/B-VII.0 k_{eff} bias is ~0.25% δk/k (270 pcm). Eight of the nine k_{eff}'s are reduced and one is unchanged with the ENDF/B-VII.1 data and the average k_{eff} bias is reduced by one-half (134 ± 115 pcm). The change in these average values is skewed by the relatively large changes for the two tungsten-bearing assemblies, ZPR-9/2 and 3, 388 ± 7 pcm and 625 ± 7 pcm, respectively. The improved k_{eff} predictions for tungsten bearing benchmarks has already been discussed and so a similar observation for calculations of the ZPR-9 assemblies is too be expected. For the other seven IEU-fueled assemblies ENDF/B-VII.1 cross sections have little effect – these assemblies were well predicted with ENDF/B-VII.0 data and remain so with the ENDF/B-VII.1 data.

Collectively the results obtained for ZPR-9 Assemblies 1-3 (shown in Fig. 18) and for ZPR-9 Assemblies 4-9 (shown in Fig. 17) provide a very strong test for tungsten in the fast energy region. The cleanest test of these data is provided with the first 4 assemblies. Assembly 1 was a well-characterized reference for these measurements. It contained no tungsten and had an enrichment (^{235}U/U) of ~11%. In Assemblies 2, 3 and 4, one-fourth, one-half, and finally all of the depleted uranium diluents in the core unit cell of Assembly 1 were replaced by tungsten – resulting in ^{235}U/U enrichments in Assemblies 2 and 3 of ~16% and ~21%, respectively. Carbon was added to the core unit cell in Assembly 5 to soften the spectrum. In Assembly 6 some of the tungsten was replaced with perforated aluminum; and in Assemblies 7, 8 and 9 the aluminum reflector was replaced with Al_2O_3 and BeO-Al. The improvement in the monotonic (or perhaps, monolithic) increase or trend in the C/E bias for Assemblies 1-4, namely, 215, 533, 897 and 1948 pcm with ENDF/B-VII.0 data, versus 205, 147, 273 and 717 pcm with ENDF/B-

VII.1 further support the changes made in the new isotopic tungsten evaluations.

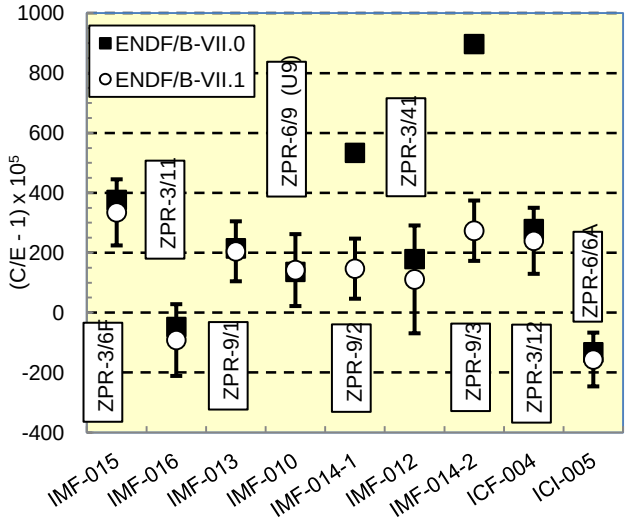

Fig 18. MCNP calculations with "As-Built" models for IEU FAST and INTER ZPR/ZPPR Assemblies.

The results shown in Fig. 19 for Mixed-(Pu, U)-fueled assemblies demonstrate that that all 14 calculated k_{eff}'s are reduced with ENDF/B-VII.1, with individual k_{eff} values dropping by approximately 60 to 215 pcm. Two of these 14 assemblies, ZPR-3/53 and ZPR-3/54, have a softer spectrum than the remaining assemblies. We note that the calculated k_{eff} biases for the ZPR-3/53 and ZPR-3/54 assemblies are considerably larger than the biases for the other twelve assemblies. The average bias for the 14 assemblies with ENDF/B-VII.0 data is 271 pcm; the average bias with ENDF/B-VII.1 is 156 pcm. The biases for ZPR-3/53 and ZPR-3/54 with ENDF/B-VII.0 data are 855 and 1233 pcm, respectively; and with ENDF/B-VII.1 data are 755 and 1047 pcm, respectively. The average bias for the other 12 assemblies with ENDF/B-VII.0 data is 142 pcm; the average bias with ENDF/B-VII.1 data is 31 pcm. In summary, the new data evaluations improve the results for the 2 softer spectrum assemblies by ~100-200 pcm; and the new data evaluations essentially remove the average bias for the remaining mixed-(Pu, U)-fueled fast assemblies.

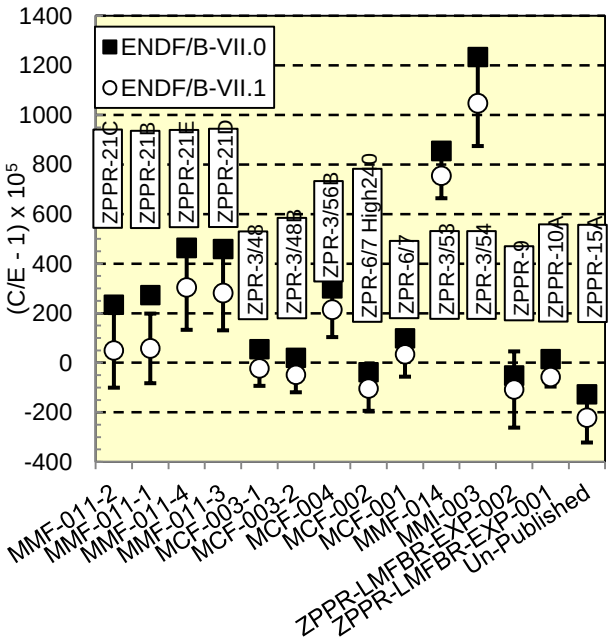

Fig. 19. MCNP Calculations with "As-Built" models for Mixed (Pu, U) FAST and INTER ZPR/ZPPR Assemblies.

There were only 2 Pu-Metal fueled experiments among the present series of detailed models of ZPR/ZPPR experiments. The first is a very fast spectrum assembly, ZPPR-21A, having ~80% of the fissions occurring above 100 keV. The C/E bias for this assembly with ENDF/B-VII.0 cross sections is 225 ± 150 pcm, which is completely eliminated, 7 ± 150 pcm, with the ENDF/B-VII.1. The second of these assemblies, ZPR-6/10, has the softest spectrum among this series of 38 assemblies, with only ~33% of the fissions occurring above 100 keV. The C/E bias for this assembly with ENDF/B-VII.0 data is ~3.8% δk (3786 ± 135 pcm), and is reduced to ~2.6% δk (2648 ± 135 pcm) with the ENDF/B-VII.1 data.

A summary comparison of the average values of C/E - 1 (in pcm) for ENDF/B-VII.1 according to Fuel Type for these 38 ZPR/ZPPR assemblies is given in Table 8. It is seen that the ENDF/B-VII.1 data consistently lower the calculated k_{eff}'s for these systems. With the exception of a few unusual assemblies in support of space nuclear (having non-traditional reflector materials) and the 3 very soft spectrum assemblies (ZPR-3/53, ZPR-3/54 and ZPR6/10) which remain badly over predicted, the tradition fast reactor assemblies are consistently well-predicted with ENDF/B-VII.1

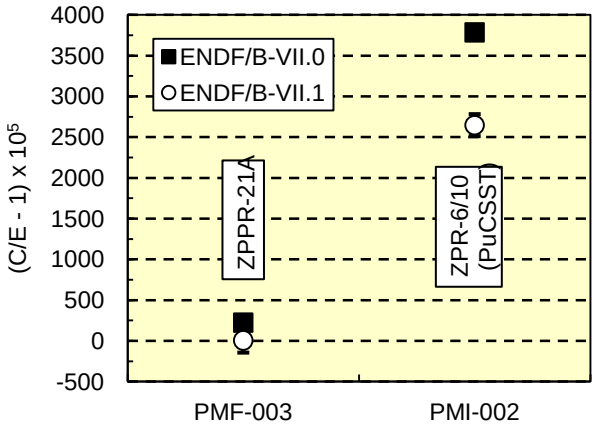

Fig. 20. MCNP Calculations with "As-Built" models for Pu metal FAST and INTER ZPR/ZPPR Assemblies.

Table 8. Summary of average calculated eigenvalue, given as k_{eff} (C/E – 1), in pcm, for ENDF/B-VII.0 and ENDF/B-VII.1. Results are categorized by ZPR/ZPPR Fuel Type.

Fuel Type	# of Expts	ENDF/B-VII.0 (C/E – 1) *	ENDF/B-VII.1 (C/E – 1) *
Pu metal **	2	2005(143)	1327(143)
Mixed (Pu, U)	14	271(114)	156(114)
HEU	13	1042(201)	463(201)
IEU	9	270(115)	134(115)

* Values in parenthesis represent the uncertainty in the corresponding least significant digits.

** Mean values are not as meaningful for this fuel type category due to the limited sample size and knowledge that the two assemblies in this category had distinctly different energy spectra.

2. *Beta-effective (β_{eff}) Measurements*

Measurements of β_{eff} were made in three of the 38 ZPR/ZPPR critical assemblies for which detailed "as-built" Monte Carlo models are available. Experimental measurements of β_{eff} were made in ZPR-9/34, ZPR-6/9 and ZPR-6/10. All 3 of these assemblies were clean, physics benchmark assemblies performed as part of the ANL Diagnostic Core Program. ZPR-9/34 (HEU-MET-INTER-001) was referred to as the Uranium/Iron Benchmark Assembly; ZPR-6/9 (IEU-MET-FAST-010) was referred to as the U9 Benchmark Assembly; and ZPR-6/10 (PU-MET-INTER-002) was referred to as the Pu/C/SST Benchmark Assembly. The beta-effective measurements in these assemblies were analyzed using these detailed models with MCNP5 and NJOY with both ENDF/B-VII.0 and -VII.1 data. Results are presented in Table 9. There is very little change in the values calculated for these 3 assemblies between ENDF/B-VII.0 and ENDF/B-VII.1 data – only the value in ZPR-6/9 is lower by ~1.5%. The calculated values are slightly higher (by 1.5 σ) than the measured values in ZPR-9/34 and in perfect agreement with the ZPR-6/9 and ZPR-6/10 measurements.

Table 9. Comparison of measured and either ENDF/B-VII.0 or ENDF/B-VII.1 calculated β_{eff} values.

Benchmark	Measured β_{eff} *	ENDF/B Version	Calculated β_{eff} *
HMI1 (ZPR-9/34, U/Fe)	0.00657(13)	VII.0 VII.1	0.00681(6) 0.00682(6)
IMF10 (ZPR-6/9, U9)	0.00706(9)	VII.0 VII.1	0.00716(6) 0.00707(6)
PMI2 (ZPR-6/10, PuC/SS)	0.00222(5)	VII.0 VII.1	0.00224(3) 0.00224(3)

* Values in parenthesis represent the uncertainty in the corresponding least significant digits.

β_{eff} was also calculated for two additional ICSBEP benchmarks, ZPR-6/6A (IEU-COMP-INTER-005) and ZPR-6/7 (MIX-COMP-FAST-001) using detailed, "as-built", Monte Carlo models, even though experimental values of β_{eff} were not available. For ZPR-6/6A the calculated β_{eff} value decreased by ~1.2% with ENDF/B-VII.1 cross sections compared to the ENDF/B-VII.0 result; for ZPR-6/7 the ENDF/B-VII.1 calculated β_{eff} value decreased by ~0.9%. Although these calculated values cannot validate either ENDF/B-VII.0 or ENDF/B-VII.1 data, they do verify that the changes from ENDF/B-VII.0 to ENDF/B-VII.1 yield only small changes in predicted β_{eff} values for typical sodium fast reactors, consistent with the small changes observed for the three assemblies (HMI1, IMF10 and PMI2) tested and discussed above.

3. *Measurements of Sodium Void Worth (ρ_{Na})*

Among the series of 38 ZPR/ZPPR critical assemblies for which detailed "as-built" Monte Carlo models are available, measurements of sodium-void worth (ρ_{Na}) were made in three, ZPPR-9, ZPPR-10A and ZPPR-15A. These measurements simulated the voiding of sodium by replacing sodium-filled stainless-steel cans with closely-matched empty stainless-steel cans from all core drawers within a specified central region. The worth of the material replacements was obtained by first measuring a sub-critical (sodium-filled) reference configuration, and then successively voiding sodium from specific regions of the core and using the Modified Source Multiplication (MSM) method to measure the sub-criticality of each voiding step. These measured reactivity changes can then be calculated by k-difference calculations using detailed Monte Carlo models of each successive assembly loading. In order to minimize the contribution of the Monte Carlo statistical uncertainties to the uncertainty in the C/E values, individual eigenvalue calculations were generally

run for 250 million histories, yielding k_{eff} stochastic uncertainties (1σ) of 2 to 3 pcm.

Results of analyzing these sodium void worth measurements with ENDF/B-VII.0 and ENDF/B-VII.1 are compared with the measured values in Table 10. Generally, these experiments were well calculated with ENDF/B-VII.0 cross sections. There is little change in calculated ρ_{Na} values using ENDF/B-VII.1, which also are generally in good agreement with the measured data.

Table 10. Comparison of sodium void worth (ρ_{Na}) measurements in ZPPR-9, ZPPR-10A and ZPPR-15A and ENDF/B-VII.0 and ENDF/B-VII.1 predictions. Measured and calculated values are in pcm.

ZPPR/Void Region	Measured ρ_{Na} *	ENDF/B Version	Calculated ρ_{Na} *
ZPPR-9			
20.32 cm axial region, 97 drawers per half	104(2)	VII.0 VII.1	106(4) 100(4)
50.80 cm axial region, 97 drawers per half	112(2)	VII.0 VII.1	109(4) 110(4)
68.58 cm axial region, 97 drawers per half	86(2)	VII.0 VII.1	85(4) 78(4)
ZPPR-10A			
20.32 cm axial region, 88 drawers per half	76(1)	VII.0 VII.1	88(4) 78(4)
20.32 cm axial region, 172 drawers per half	145(2)	VII.0 VII.1	153(4) 148(4)
40.64 cm axial region, 172 drawers per half	187(2)	VII.0 VII.1	194(4) 192(4)
50.80 cm axial region, 172 drawers per half	159(2)	VII.0 VII.1	160(4) 154(4)
ZPPR-15A			
20.32 cm axial region, 148 drawers per half	370(3)	VII.0 VII.1	352(4) 356(4)
35.56 cm axial region, 148 drawers per half	101(1)	VII.0 VII.1	89(4) 80(4)
45.72 cm axial region, 148 drawers per half	-35(1)	VII.0 VII.1	-39(4) -30(4)
78.74 cm axial region, 148 drawers per half	-76(2)	VII.0 VII.1	-75(4) -84(4)

* Values in parenthesis represent the uncertainty in the corresponding least significant digits.

4. Worth Measurements of Control Rods and Control Positions

Worth measurements of simulated control rods (CRs) and control rod positions (CRPs) were also made in the ZPPR-9, ZPPR-10A and ZPPR-15A assemblies. As with the measurement of the sodium void worths, these experiments were performed by first measuring a sub-critical reference configuration and then using the MSM method to measure the sub-criticality of subsequent configurations containing simulated CRs and/or CRPs.

Results of analyzing these control rod and control rod position worth measurements with ENDF/B-VII.0 and ENDF/B-VII.1 cross sections are presented in Table 11. As for the sodium void measurements, these control rod experiments are generally well calculated with ENDF/B-VII.0. And again there is very little change in the calculated values using with the ENDF/B-VII.1, which also are generally in good agreement with the measured data. The ZPPR-10A measurements are slightly over-predicted and the ZPPR-15A measurements are slightly under-predicted. However, in both cases the changes obtained between the ENDF/B-VII.0 and ENDF/B-VII.1 data are smaller than the uncertainties in the measurements.

Table 11. Comparison of Control Rod (CR) and Control Rod Position (CRP) measurements in ZPPR-9, ZPPR-10A and ZPPR-15A and ENDF/B-VII.0 and ENDF/B-VII.1 predictions. Measured and calculated values are in pcm.

ZPPR/CR or CRP	Measured ρ_{CR} *	ENDF/B Version	Calculated ρ_{CR} *
ZPPR-9			
6 CRs, row 7	-969(12)	VII.0 VII.1	-991(4) -980(4)
6 CRPs, row 7	-6245(73)	VII.0 VII.1	-6356(5) -6379(5)
6 CRs in center and middle ring	-6131(74)	VII.0 VII.1	-6170(5) -6198(5)
CRs 4 and 7	-2315(28)	VII.0 VII.1	-2374(4) -2372(4)
Central 3x3 CR	-1179(14)	VII.0 VII.1	-1209(4) -1209(4)
ZPPR-10A			

Central Rod	-886(10)	VII.0 VII.1	-945(9) -953(4)
6 CRs, row 4	-4496(48)	VII.0 VII.1	-4833(4) -4854(4)
12 CRs, row 7	-7156(105)	VII.0 VII.1	-7550(5) -7574(5)
6 row 7 corner rods	-3237(37)	VII.0 VII.1	-3447(4) -3458(4)
ZPPR-15A			
Central 2x2 Na CRP	-161(2)	VII.0 VII.1	-160(4) -156(4)
Central 2x2 CR – 100% $^{nat}B_4C$	-1306(9)	VII.0 VII.1	-1265(4) -1277(4)
Central 2x2 CR – 50% $^{nat}B_4C$	-999(7)	VII.0 VII.1	-910(4) -932(4)
* Values in parenthesis represent the uncertainty in the corresponding least significant digits.			

In summary, the analysis of the detailed Monte Carlo models for this series of fast reactor systems with ENDF/B-VII.1 data confirms the analysis performed using the simplified ICSBEP benchmarks for these systems. Prediction of criticality is generally improved with the new data, and select new evaluations such as tungsten are considerably improved. Analyses of β_{eff}, sodium-void worth and control rod worth measurements confirmed that the new data make only small changes in these parameters, and the generally good performance of ENDF/B-VII.0 will be maintained with ENDF/B-VII.1 data.

G. Reaction Rate Studies

Advanced nuclear systems and associated fuel cycles need accurate cross section data to provide a reliable assessment of their performance. Closed fuel cycles with the objective of waste minimization imply, from a physics point of view:

- A high content of minor actinides in the reactor core and in the fuel cycle;
- A high Fissile/Fertile isotope content in the core fuel;
- A variable, and potentially degraded, Pu isotopic vector in the fuel cycle;
- Lower fuel density to achieve lower conversion ratios

Basic data are available for TRU (transuranic) isotopes (up to Cf) but a validation is needed in order to quantify their reliability. The high amount of minor actinides (MA) foreseen in advanced fuel cycle systems requires specific validation work, especially for capture and fission cross sections of such isotopes.

Such validation is traditionally done through the use of differential and integral experiments, and uncertainty assessment. Information that can be gathered on MA's from experiment comes mostly from small sample irradiation, reactivity oscillation, and fission and capture rate measurements. Separate isotope sample and fuel pin irradiation in power reactors also provides a unique source of measurement data.

Results from analyses of such experiments provide indications to nuclear data evaluators for improving the quality of basic files, and to assess their impact on advanced fuel cycles. Experimental data from the PROFIL and TRAPU irradiation experiments [7], performed at the CEA PHENIX fast reactor, provide clean and precise information on both cross section data and transmutation rates of actinides. These data are essential for the validation of the methods and data to be used in advanced fuel cycles where transmutation systems will be used to reduce the existing inventory of nuclear waste.

During the PROFIL-1 experiment (see Fig. 21), performed in 1974, a pin containing 46 samples, including fission products plus major and minor actinides (Uranium, Plutonium, and Americium isotopes) was irradiated in the PHENIX reactor for the first three cycles, corresponding to a total of 189.2 full-power days. The experimental pin was located in the central subassembly of the core, and in the third row of pins inside the subassembly. This location is far away from neutronic perturbations allowing clear irradiation conditions. Following the reactor irradiation, mass spectroscopy was then used, with simple or double isotopic dilution and well-characterized tracers to measure isotopic concentrations. The experimental uncertainty obtained with this method is relatively small.

The second part of the PROFIL irradiation campaign took place in 1979. During this experiment two standard pins, each containing 42 separated capsules of fission products plus major and minor actinides (Uranium, Plutonium, Americium and Neptunium isotopes), were irradiated for four cycles (the 17th through 20th) in the PHENIX reactor. As for PROFIL-1, chemical and mass spectrometry analyses have been subsequently performed to determine the post-irradiation isotopic concentrations.

The TRAPU experiment consisted of a six-cycle irradiation (10th to 15th) of mixed-oxide pins containing plutonium of different isotopic compositions but heavily loaded in the higher isotopes ($^{240,241,242}Pu$) compared to typical PHENIX fuel. Three types of plutonium containing pins were used.

After irradiation, 20 mm tall samples were cut from the pins (both fuel and clad) and put into a solution in order to determine the fuel composition by nuclide. ^{148}Nd was used as a burn-up indicator as it is a stable fission product with a small capture cross section, thereby enabling accurate determination of the number of fission reactions that took place in the sample. Again, isotopic data were obtained using mass spectrometry techniques, with simple or double isotopic dilution and well-characterized tracers.

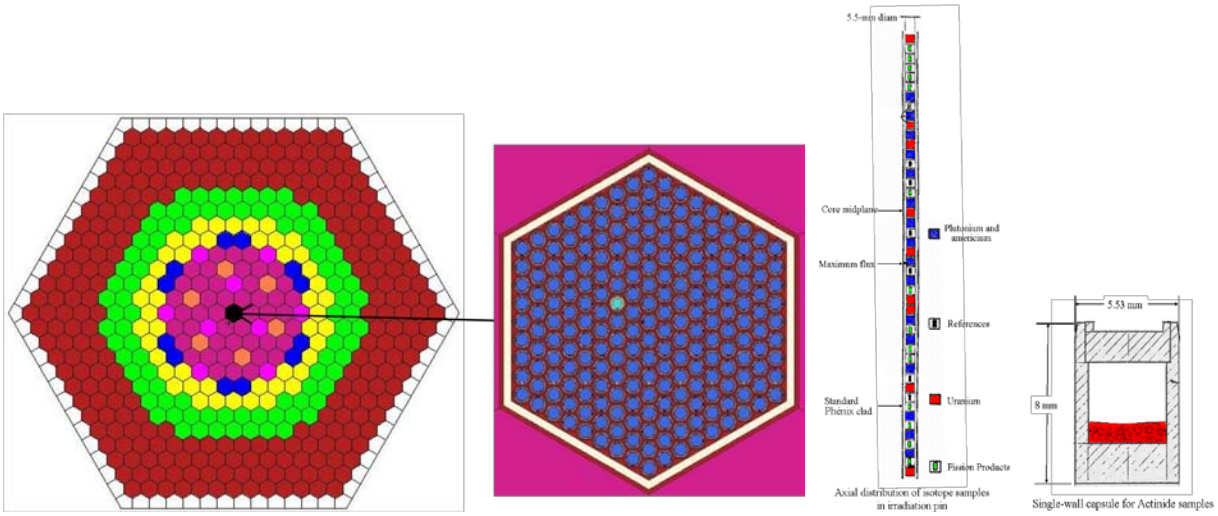

Fig. 21. PROFIL-1 irradiation experiment in the French fast reactor PHENIX.

MCNP5 models were developed for the analysis of the irradiation experiments. One group cross sections for the samples were calculated by taking batch statistics of several independent calculations with recorded surface sources. For the results obtained using ENDF/B-VII.1 data, the same recorded surfaces histories obtained with ENDF/B-VII.0 data were used. This assumption is justified as the cross section data for the major actinides comprising the PHENIX reactor fuel did not change significantly between ENDF/B-VII.0 and VII.1.

Tables 12 and 13 show a comparison of the C/E's for the different irradiation experiments (PROFIL-1 and PROFIL-2 in Table 12, TRAPU-1, -2 and -3 in Table 13). In the PROFIL experiments improvements can be observed for the ENDF/B-VII.1 capture data in ^{238}Pu, ^{241}Am, ^{244}Cm, ^{97}Mo, ^{151}Sm, ^{153}Eu, and for ^{240}Pu(n,2n). On the other hand, ^{240,242}Pu, ^{95}Mo, ^{133}Cs and ^{145}Nd capture C/E results are worse. For the major actinides ^{235}U and especially ^{239}Pu capture C/E's are underestimated. For fission products, ^{105,106}Pd, ^{143,144}Nd and ^{147,149}Sm are significantly underestimated, while ^{101}Ru and ^{151}Sm are overestimated. Other C/E deviations from unity are within the combined experimental and calculated statistical uncertainty.

Table 12. C/E's for the PROFIL-1 and PROFIL-2 irradiation experiments.

Data Type	PROFIL-1 C/E		
	VII.0	**VII.1**	**Exp. Unc.**
σ_{capt} ^{235}U	0.948	0.948	1.7 %
σ_{capt} ^{238}U	0.972	0.972	2.3 %
σ_{capt} ^{238}Pu	1.299	1.135	4.0 %
σ_{capt} ^{239}Pu	0.906	0.906	3.0 %
$\sigma_{n,2n}$ ^{239}Pu	0.745	0.745	15.0 %
σ_{capt} ^{240}Pu	0.964	0.945	2.2 %
$\sigma_{n,2n}$ ^{240}Pu	0.779	1.084	15.0 %
σ_{capt} ^{241}Pu	0.950	0.947	4.1 %
σ_{capt} ^{242}Pu	1.061	1.120	3.5 %
σ_{capt} ^{241}Am	0.968	0.984	1.7 %
σ_{capt} ^{243}Am	0.834	0.834	5.0 %
σ_{capt} ^{95}Mo	1.032	1.063	3.8 %
σ_{capt} ^{97}Mo	0.968	0.993	4.4 %
σ_{capt} ^{101}Ru	1.101	1.095	3.6 %
σ_{capt} ^{105}Pd	0.852	0.845	4.0 %
σ_{capt} ^{133}Cs	0.878	0.827	4.7 %
σ_{capt} ^{145}Nd	0.955	0.936	3.8 %
σ_{capt} ^{149}Sm	0.915	0.908	3.1 %
	PROFIL-2 C/E		
	VII.0	**VII.1**	**Exp. Unc.**
σ_{capt} ^{235}U	0.967	0.967	1.7 %
σ_{capt} ^{238}U	0.985	0.985	2.3 %
σ_{capt} ^{237}Np	0.944	0.941	3.6 %
σ_{capt} ^{238}Pu	1.341	1.181	4.0 %
σ_{capt} ^{239}Pu	0.922	0.922	3.0 %
$\sigma_{(n,2n)}$ ^{239}Pu	0.574	0.574	15.0%
σ_{capt} ^{240}Pu	0.973	0.961	2.2 %
σ_{capt} ^{242}Pu	1.054	1.114	4.3 %
σ_{capt} ^{241}Am	1.018	1.029	1.7 %
σ_{capt} ^{244}Cm	1.101	0.956	2.0 %
σ_{capt} ^{106}Pd	0.939	0.939	2.0 %
σ_{capt} ^{143}Nd	0.937	0.937	2.0 %
σ_{capt} ^{144}Nd	0.935	0.928	2.0 %
σ_{capt} ^{147}Sm	0.894	0.894	2.0 %
σ_{capt} ^{151}Sm	1.094	1.085	2.0 %
σ_{capt} ^{153}Eu	0.924	0.954	2.0 %

From the TRAPU analysis, the major improvement is in the predicted ^{243}Cm build-up, presumably due to an improved ^{242}Cm capture evaluation.

Table 13. C/E's for the TRAPU-1, TRAPU-2 and TRAPU-3 irradiation experiments.

Isotope	TRAPU-1 C/E		
	VII.0	VII.1	Exp. Unc.
^{234}U	1.006	1.004	± 3.9 %
^{235}U	1.001	1.002	± 0.4%
^{236}U	0.972	0.971	± 0.8 %
^{237}Np	0.970	0.879	± 6.8 %
^{238}Pu	1.004	0.992	± 1.5 %
^{239}Pu	1.031	1.034	± 0.6 %
^{240}Pu	1.003	1.007	± 0.6 %
^{241}Pu	1.011	1.004	± 0.6 %
^{242}Pu	1.036	1.028	± 0.8 %
^{241}Am	0.979	0.975	± 3.2 %
^{242m}Am	1.009	1.016	± 3.8 %
^{243}Am	0.978	1.025	± 2.6 %
^{242}Cm	1.035	0.984	± 3.9 %
^{243}Cm	-	-	-
^{244}Cm	0.843	0.882	± 2.1 %
	TRAPU-2 C/E		
	VII.0	VII.0	VII.0
^{234}U	1.023	1.026	± 3.8 %
^{235}U	1.020	1.021	± 0.4 %
^{236}U	0.995	0.992	± 1.0 %
^{237}Np	0.963	0.988	± 3.3 %
^{238}Pu	0.990	0.998	± 1.0 %
^{239}Pu	1.012	1.014	± 0.5 %
^{240}Pu	0.984	0.985	± 0.6 %
^{241}Pu	0.992	0.988	± 0.6 %
^{242}Pu	1.010	1.003	± 0.6 %
^{241}Am	0.986	0.983	± 3.9 %
^{242m}Am	1.039	1.049	± 4.3 %
^{243}Am	0.959	1.010	± 3.1 %
^{242}Cm	1.017	0.964	± 3.1 %
^{243}Cm	0.483	1.104	± 3.1 %
^{244}Cm	0.946	0.996	± 2.3 %
	TRAPU-3 C/E		
	VII.0	VII.0	VII.0
^{234}U	1.065	1.067	± 4.6 %
^{235}U	1.019	1.019	± 0.4 %
^{236}U	0.992	0.991	± 0.9 %
^{237}Np	0.908	0.915	± 3.2 %
^{238}Pu	1.013	1.001	± 1.6 %
^{239}Pu	1.018	1.020	± 0.4 %
^{240}Pu	0.998	1.002	± 0.6 %
^{241}Pu	1.004	0.999	± 0.6 %
^{242}Pu	1.009	1.003	± 0.6 %
^{241}Am	0.991	0.987	± 2.6 %
^{242m}Am	1.021	1.031	± 3.1%
^{243}Am	1.000	1.050	± 2.5 %
^{242}Cm	1.011	0.959	± 2.7 %
^{243}Cm	0.490	1.106	± 3.2 %
^{244}Cm	0.961	1.009	± 1.8 %

The PROFIL and TRAPU experiments can also provide information on fission cross sections. In the case of PROFIL the experimental results provide the Nd isotope build-up in the actinide samples. If the fission product yield is well known, an estimate can be made for the fission cross section. Nevertheless, the knowledge of the fission yields is based on the fission cross sections, so this can be a tautological situation. In the case of TRAPU, the fission information comes through the sensitivity to this cross section to the buildup of the isotopes.

A more accurate way to gather information on fission cross sections from elemental experiments is through the analysis of fission spectral indices. In this case, fission reaction rates of actinides are measured against a standard, in particular ^{235}U fission. If the measurements are done in the center of a reactor in a well characterized spectrum, indirect effects are minimal and the result can be directly related to the actinide fission cross section. This is the situation for the COSMO experimental campaign, performed at the French zero power fast spectrum facility MASURCA, where different actinide fission spectral indices were measured. The experiment was analyzed based upon the benchmark specifications provided in Ref. [8] and results are shown in Table 14. We conclude from these results that ENDF/B-VII.1 ^{238,240}Pu fission cross sections have improved while ^{242}Pu's fission cross section has not.

Table 14. C/E's for COSMO fission spectral indices

Isotope	COSMO C/E		
	VII.0	VII.1	Exp. Unc.
σ_{fis} ^{238}U	0.984	0.981	1.5 %
σ_{fis} ^{237}Np	1.005	1.004	1.5 %
σ_{fis} ^{238}Pu	1.072	1.040	2.5 %
σ_{fis} ^{239}Pu	0.991	0.989	1.3%
σ_{fis} ^{240}Pu	1.051	1.028	2.3 %
σ_{fis} ^{241}Pu	1.004	1.001	2.0 %
σ_{fis} ^{242}Pu	1.018	1.041	2.3 %
σ_{fis} ^{241}Am	1.089	1.081	2.3 %
σ_{fis} ^{243}Am	1.010	1.009	2.3 %

Additional reaction rate data are available from the ICSBEP Handbook's FUND-IPPE-RR-MULT-RRR-001 benchmark. This is an unmoderated, Pu fueled assembly with a central cavity for sample irradiation. As with any reactor based measurement the flux spectrum seen by the sample covers a broad energy distribution. In these measurements the average energy of that spectrum is near 1.5 MeV. A number of actinide and structure cross section ratio measurements have been reported. As with the PROFIL, TRAPU and COSMO experiments above the data are given as a spectral index, again to ^{235}U(n,f). Measured and calculated results are given in Tables 15 and 16.

Table 15. Measured and calculated spectral indices for selected actinide cross sections from the FUND-IPPE-RR-MULT-RRR-001 benchmark. Values in parenthesis

represent the uncertainty in the corresponding least significant digits.

Reaction	Model Value	ENDF/B-VII.0	ENDF/B-VII.1
^{232}Th(n,f)	0.0430(13)	0.0398(2)	0.0399(1)
^{233}U(n,f)	1.54(3)	1.5546(7)	1.5544(1)
^{234}U(n,f)	0.790(24)	0.7294(4)	0.7293(1)
^{236}U(n,f)	0.333(10)	0.3215(2)	0.3216(1)
^{238}U(n,f)	0.165(5)	0.1622(1)	0.1622(1)
^{237}Np(n,f)	0.771(23)	0.8135(4)	0.8134(1)
^{239}Pu(n,f)	1.33(4)	1.3603(6)	1.3602(1)
^{240}Pu(n,f)	0.877(26)	0.8234(4)	0.8110(1)
^{241}Pu(n,f)	1.29(4)	1.3222(6)	1.3219(1)
^{242}Pu(n,f)	0.658(20)	0.6704(4)	0.6859(1)
^{241}Am(n,f)	0.825(25)	0.7816(4)	0.7782(1)

Many of the major actinide cross sections are little or unchanged in ENDF/B-VII.1 compared to ENDF/B-VII.0; a notable exception being ^{236}U whose ENDF/B-VII.0 capture cross section is clearly low. The upward revision found in ENDF/B-VII.1 yields a clearly superior C/E value.

Table 16. Measured and calculated spectral indices for selected structural element cross sections from the FUND-IPPE-RR-MULT-RRR-001 Benchmark. Values in parenthesis represent the uncertainty in the corresponding least significant digits.

Reaction	Model Value	ENDF/B-VII.0	ENDF/B-VII.1
^{27}Al(n,α)	0.00043(2)	0.00046(1)	0.00046(1)
^{54}Fe(n,α)	0.00050(2)	0.00053(1)	0.00053(1)
^{59}Co(n,α)	0.000095(4)	0.000096(1)	0.000095(1)
^{92}Mo(n,α)	0.000055(5)	0.000086(1)	0.000085(1)
^{24}Mg(n,p)	0.00090(4)	0.00102(1)	0.00101(1)
^{27}Al(n,p)	0.00221(15)	0.00205(1)	0.00215(1)
^{46}Ti(n,p)	0.0066(3)	0.0071(1)	0.0058(1)
^{47}Ti(n,p)	0.0097(5)	0.0093(1)	0.0102(1)
^{48}Ti(n,p)	0.000180(8)	0.000180(1)	0.000219(1)
^{54}Fe(n,p)	0.0447(15)	0.0418(1)	0.0418(1)
^{56}Fe(n,p)	0.00061(2)	0.00062(1)	0.00061(1)
^{58}Ni(n,p)	0.055(3)	0.0552(1)	0.0553(1)
^{59}Co(n,p)	0.00084(4)	0.00078(1)	0.00078(1)
^{50}Cr(n,γ)	0.0057(5)	0.0055(1)	0.0052(1)
^{55}Mn(n,γ)	0.00297(15)	0.00386(1)	0.00391(1)
^{58}Fe(n,γ)	0.00228(9)	0.00302(1)	0.00299(1)
^{59}Co(n,γ)	0.0064(3)	0.0059(1)	0.0059(1)
^{64}Ni(n,γ)	0.00185(8)	0.00475(1)	0.00353(1)
^{63}Cu(n,γ)	0.0114(5)	0.0120(1)	0.0120(1)
^{65}Cu(n,γ)	0.0076(6)	0.0075(1)	0.0075(1)
^{98}Mo(n,γ)	0.0193(8)	0.0271(1)	0.0271(1)
^{94}Zr(n,γ)	0.0064(4)	0.0096(1)	0.0096(1)
^{96}Zr(n,γ)	0.00306(15)	0.00475(10)	0.00464(10)
^{197}Au(n,γ)	0.105(5)	0.101(1)	0.101(1)

These results have not been generally available to the evaluation community before. It is our expectation that the results provided herein will be judged useful as revised evaluation efforts are undertaken in the future.

H. Rossi-α

Rossi-α characterizes the exponential change in the population of prompt neutrons that produce fissions in a system that is close to delayed critical:

$$n_{pf}(t) = n_{pf0}e^{\alpha_R t}$$

where α_R is Rossi-α, n_{pf} is the population of prompt neutrons that produce fissions, and t is time. By definition, Rossi-α is zero at prompt critical, negative below it, and positive above it. It is straightforward to show that

$$\alpha_R = \frac{k_p - 1}{\Lambda_{pf}} \cong - \frac{\beta_{eff}}{\Lambda_{pf}}$$

where k_p is the prompt neutron multiplication factor, Λ_{pf} is the lifetime for prompt neutrons producing fission, and β_{eff} is the effective delayed neutron fraction. A technique to measure Rossi-α using correlated fission chains was developed by Bruno Rossi in the 1950s [9].

Version 1.60 of the MCNP5 Monte Carlo code, released from RSICC in November 2010, is capable of computing Rossi-α in criticality calculations [10]. As part of the validation of that capability, a Rossi-α validation suite has been developed. This suite includes ^{233}U, HEU, IEU, and plutonium benchmarks. These benchmarks include systems with thermal, intermediate, and fast spectra. Some of the benchmarks are unreflected, while the others are reflected by normal uranium, depleted uranium, thorium, copper or water. Summary descriptions of the 13 benchmarks in the suite are given in Table 17.

Table 17. Benchmarks in the Rossi-α benchmark suite. Refer to the ICSBEP Handbook for additional details.

Fuel	Name	Spectrum	ICSBEP Handbook Identifier
^{233}U	Jezebel-23	Fast	U233-MET-FAST-001
	Flattop-23	Fast	U233-MET-FAST-006
HEU	Godiva	Fast	HEU-MET-FAST-001
	Flattop-25	Fast	HEU-MET-FAST-028
	Zeus-1	Inter	HEU-MET-INTER-006
	Zeus-5	Fast	HEU-MET-FAST-073
	Zeus-6	Fast	HEU-MET-FAST-072
IEU	Big-10	Fast	IEU-MET-FAST-007
	STACY-30	Thermal	LEU-SOL-THERM-007
	STACY-46	Thermal	LEU-SOL-THERM-004
Pu	Jezebel	Fast	PU-MET-FAST-001
	Flattop-Pu	Fast	PU-MET-FAST-006
	THOR	Fast	PU-MET-FAST-008

The measured values of Rossi-α for all but five of the benchmarks are taken from the CSEWG Benchmark Book [11]. Measured values for STACY-30 and STACY-46 are taken from Reference [12]. The measured value for Zeus-1 is taken from the ICSBEP Handbook while the values for Zeus-5 and Zeus-6 are taken from the logbooks for those experiments.

Calculated results using ENDF/B-VII.0 and ENDF/B-VII.1 cross sections are presented in Table 18.

Table 18. Comparison of measured and calculated values for Rossi-α.

Benchmark	Rossi-α (10^4 generations/second) at Delayed Critical		
	Measured	MCNP5-1.60 Results	
		ENDF/B-VII.0	ENDF/B-VII.1
Jezebel-23	-100 ± 1	-108 ± 1	-102 ± 9
Flattop-23	-26.7 ± 0.5	-30.2 ± 0.4	-28.9 ± 2.4
Godiva	-111 ± 2	-113 ± 2	-121 ± 8
Flattop-25	-38.2 ± 0.2	-39.7 ± 0.2	-38.5 ± 2.6
Zeus-1	-0.338 ± 0.008	-0.363 ± 0.002	-0.352 ± 0.023
Zeus-5	-14.8 ± 0.1	-10.8 ± 0.1	-10.8 ± 0.7
Zeus-6	-3.73 ± 0.05	-4.14 ± 0.03	-4.10 ± 0.26
Big-10	-11.7 ± 0.1	-11.8 ± 0.1	-11.5 ± 0.7
STACY-30	-0.0127 ± 0.0003	-0.0133 ± 0.0003	-0.0130 ± 0.0010
STACY-46	-0.0106 ± 0.0004	-0.0104 ± 0.0002	-0.0103 ± 0.0008
Jezebel	-64 ± 1	-65 ± 1	-71 ± 9
Flattop-Pu	-21.4 ± 0.5	-21.0 ± 0.3	-21.3 ± 2.2
THOR	-19 ± 1	-20 ± 1	-22 ± 2

ENDF/B-VII.1 delayed neutron data have reverted to what had been available in ENDF/B-VI.8; a revision generally supported by these calculations.

III. Conclusions

Hundreds of criticality benchmarks from the ICSBEP Handbook have been calculated with one or more of ENDF/B-VI.8, ENDF/B-VII.0 and ENDF/B-VII.1 cross sections in a comprehensive test of the underlying neutron cross section data. These studies have demonstrated that the new cross section library, ENDF/B-VII.1, is an important advance over the predecessor library, ENDF/B-VII.0. Accurate k_{eff} predictions are obtained for a wide variety of critical benchmark assemblies for all fissile nuclides of interest under all spectral conditions from bare unmoderated assemblies to highly moderated assemblies. Significant advances in the underlying accuracy of the basic neutron cross section evaluations have occurred with each ENDF/B generation, and we continue to retain the highly accurate results obtained with past ENDF/B files for unmoderated bare and uranium reflected ^{233,235}U and ^{239}Pu systems (e.g., Godiva, Jezebel, Flattop's and Big-10). Previous highly accurate criticality predictions for HEU solution systems and low-enriched lattices are also retained. Deficiencies identified since the release of ENDF/B-VII.0 for several elements have been eliminated; most notably for unmoderated systems with metallic titanium and tungsten reflectors. Nevertheless, further improvements await future ENDF/B releases. Our benchmark simulations for beryllium and vanadium reflected systems do not yield the same level of accuracy. Beryllium in particular is problematic as different benchmark suites with many common components yield C/E k_{eff} values that vary by more than 0.5% - a reasonably accurate standard in the past but with today's computational resources and measurement and evaluation techniques we expect better. New experiments are planned in coming years with the expectation that this issue will be resolved. Other long-standing issues, such as the overpredicted k_{eff} values for Pu solution systems and the apparent k_{eff} trend in ^{233}U systems noted above also remain. We close by noting that these are not new deficiencies, rather they have exist in all internationally available evaluated nuclear data files, as well as in earlier ENDF/B libraries. The ENDF/B-VII.1 library represents the most accurate general purpose nuclear data file yet produced by the Cross Section Evaluation Working Group community.

Acknowledgements

We gratefully acknowledge valuable discussions …

References

[1] M.B.Chadwick et al, "ENDF/B-VII.0: Next Generation Evaluated Nuclear Data Library for Nuclear Science and Technology," *Nuclear Data Sheets*, **107**, 2931-3060 (2006).

[2] M.B.Chadwick et al, "ENDF/B-VII.1 Nuclear Data for Science and Technology: Cross Sections, Covariances, Fission Product Yields and Decay Data," *Nuclear Data Sheets* **112**, xxx (2011, this issue).

[3] R.E.MacFarlane and A.C.Kahler, "Methods for Processing ENDF/B-VII with NJOY," *Nuclear Data Sheets*, vol. 111, 2739 – 2890 (2010).

[4] X-5 Monte Carlo Team, "MCNP – A General Monte Carlo Transport Code, Version 5," Los Alamos National Laboratory report LA-UR-03-1987 (April 2003).

[5] J.B.Briggs, editor, "International Handbook of Evaluated Criticality Safety Benchmark Experiments," Technical Report NEA/NSC/DOC(95)03, Nuclear Energy Agency, Paris, France, 2010. This Handbook is updated

annually. Benchmark models used herein come from the 2005 and later editions.

[6] Y.Daron, R.C.Block, M.J.Rapp, F.J.Saglime, G.Leinweber, D.P.Barry, N.J.Drindak and J.G.Hoole, "Beryllium and Graphite High Accuracy Total Cross Section Measurements in the Energy Range from 24 to 900 keV," *Nucl. Sci. and Eng*. **161**, 321-330 (2009).

[7] A.D'Angelo, F.Cleri, P.Marimbeau, M.Salvatores and J.P.Grouiller, "Analysis of Sample and Fuel Pin Irradiation in PHENIX for Basic Nuclear Data Validation", *Nucl. Sci. and Eng*. **105**, 244.

[8] "Benchmark on Computer Simulation of MASURCA Critical and Subcritical Experiments", NEA/NSC/DOC(2005)23.

[9] J. Orndoff, "Prompt Neutron Periods of Metal Critical Assemblies," *Nucl. Sci. Eng.,* **2**, 450-460 (July 1957).

[10] B. Kiedrowski, F.B.Brown and P.Wilson, "Calculating Kinetics Parameters and Reactivity Changes with Continuous Energy Monte Carlo," *Proceedings of PHYSOR 2010.* Pittsburgh, Pa 2010.

[11] *Cross Section Evaluation Working Group Benchmark Specifications*, Brookhaven National Laboratory report BNL-19302, ENDF-202 (Rev., September 1986).

[12] K. Tonoike, Y. Miyoshi, T. Kikuchi, and T. Yamamoto, "Kinetic Parameter β_{eff}/ℓ Measurement on Low Enriched Uranyl Nitrate Solution with Single Unit Cores (600φ, 280T, 800φ) of STACY," *J. Nucl. Sci. Tech.*, **39**, 11, 1227-1236 (November 2002).

Appendix A

Tabulated below are the calculated eigenvalues for a subset of the ICSBEP Benchmarks discussed elsewhere in this paper. These results were obtained after independent benchmark model development, independent cross section processing into the appropriate application library and with independently developed transport codes – MCNP and Tripoli.

The high degree of agreement in these calculations provides added confidence in the general conclusions on the strengths and weaknesses of the ENDF/B-VII.1 library that were presented in the main body of this paper.

Table A1. Independent MCNP5 and Tripoli-4.7 k_{eff} calculations using ENDF/B-VII.1 cross sections

Benchmark	**Model k_{eff}**	**ENDF/B-VII.1 MCNP Calculated k_{eff}**	**ENDF/B-VII.1 Tripoli-4.7 Calculated k_{eff}**
HEU-MET-FAST-001 (Godiva)	1.0000(10)	0.99980(8)	1.00014(11)
HEU-MET-FAST-028 (Flattop)	1.0000(30)	1.00298(9)	1.00325(11)
PU-MET-FAST-001 (Jezebel)	1.0000(20)	0.99988(8)	0.99960(15)
PU-MET-FAST-002	1.0000(20)	1.00002(8)	0.99975(15)
IEU-MET-FAST-001.2	1.0000(12)	1.00047(9)	0.99850(12)
IEU-MET-FAST-001.3	1.0000(10)	1.00099(9)	1.00056(12)
IEU-MET-FAST-001.4	1.0000(10)	1.00159(9)	1.00132(12)
IEU-MET-FAST-002	1.0000(30)	0.99883(8)	0.99912(10)
IEU-MET-FAST-007 (Big-10, detailed and CSEWG two-zone models)	1.0045(7) 0.9948(13)	1.00440(7) 0.99502(7)	1.00479(13) 0.99515(13)
IEU-MET-FAST-010	0.9954(24)	0.99624(10)	0.99710(13)
IEU-MET-FAST-012	1.0007(27)	1.00329(10)	1.00370(13)
HEU-SOL-THERM-001.1	1.0004(60)	0.99794(15)	0.99965(16)
HEU-SOL-THERM-001.2	1.0021(72)	0.99595(15)	0.99766(16)
HEU-SOL-THERM-001.3	1.0003(35)	1.00193(15)	1.00304(16)
HEU-SOL-THERM-001.4	1.0008(53)	0.99841(15)	0.99958(16)
HEU-SOL-THERM-001.5	1.0001(49)	0.99871(13)	0.99966(16)
HEU-SOL-THERM-001.6	1.0002(46)	1.00202(13)	1.00292(16)
HEU-SOL-THERM-001.7	1.0008(40)	0.99793(15)	0.99878(16)

HEU-SOL-THERM-001.8	0.9998(38)	0.99803(15)	0.99961(16)
HEU-SOL-THERM-001.9	1.0008(54)	0.99428(15)	0.99549(16)
HEU-SOL-THERM-009.1	0.9990(43)	1.00297(14)	1.00316(16)
HEU-SOL-THERM-009.2	1.0000(39)	1.00306(14)	1.00338(16)
HEU-SOL-THERM-009.3	1.0000(39)	1.00242(14)	1.00294(16)
HEU-SOL-THERM-009.4	0.9986(35)	0.99669(14)	0.99726(16)
HEU-SOL-THERM-011.1	1.0000(23)	1.00466(12)	1.00527(16)
HEU-SOL-THERM-011.2	1.0000(23)	1.00100(11)	1.00182(16)
HEU-SOL-THERM-012	0.9999(58)	1.00084(8)	1.00102(15)
HEU-SOL-THERM-032	1.0015(26)	0.99933(5)	0.99892(16)
PU-SOL-THERM-001.1	1.0000(50)	1.00612(13)	1.00645(12)
PU-SOL-THERM-001.2	1.0000(50)	1.00761(13)	1.00819(12)
PU-SOL-THERM-001.3	1.0000(50)	1.01049(13)	1.01104(12)
PU-SOL-THERM-001.4	1.0000(50)	1.00443(13)	1.00520(12)
PU-SOL-THERM-001.5	1.0000(50)	1.00863(13)	1.00920(12)
PU-SOL-THERM-001.6	1.0000(50)	1.00957(13)	1.01055(12)
PU-SOL-THERM-009.3	1.0003(33)	1.01928(6)	1.01923(11)
PU-SOL-THERM-011 (16.1)	1.0000(52)	1.01020(13)	1.01017(13)
PU-SOL-THERM-011 (16.5)	1.0000(52)	1.00628(13)	1.00665(13)
PU-SOL-THERM-011 (18.1)	1.0000(52)	0.99462(11)	0.99449(13)
PU-SOL-THERM-011 (18.6)	1.0000(52)	1.00024(12)	1.00044(13)
LEU-COMP-THERM-006.1	1.0000(20)	1.00004(10)	1.00074(12)
LEU-COMP-THERM-006.3	1.0000(20)	1.00034(10)	1.00114(9)
LEU-COMP-THERM-006.4	1.0000(20)	0.99989(10)	1.00092(12)
LEU-COMP-THERM-006.8	1.0000(20)	1.00004(10)	1.00086(12)
LEU-COMP-THERM-006.9	1.0000(20)	1.00003(10)	1.00053(12)
LEU-COMP-THERM-006.13	1.0000(20)	0.99954(10)	1.00010(12)
LEU-COMP-THERM-006.14	1.0000(20)	0.99952(10)	1.00052(12)
LEU-COMP-THERM-006.18	1.0000(20)	0.99961(10)	1.00005(12)
LEU-COMP-THERM-007.1	1.0000(16)	0.99761(11)	0.99851(10)
LEU-COMP-THERM-007.2	1.0000(16)	0.99880(11)	0.99984(10)
LEU-COMP-THERM-007.3	1.0000(16)	0.99766(10)	0.99842(10)
LEU-COMP-THERM-007.5	1.0000(16)	0.99714(11)	0.99843(10)
LEU-COMP-THERM-007.6	1.0000(16)	0.99883(10)	1.00003(10)
LEU-COMP-THERM-007.7	1.0000(16)	0.99834(10)	0.99942(10)
LEU-COMP-THERM-039.1	1.0000(14)	0.99722(11)	0.99815(12)
LEU-COMP-THERM-039.4	1.0000(14)	0.99635(11)	0.99746(12)
LEU-COMP-THERM-039.6	1.0000(14)	0.99729(11)	0.99824(12)
LEU-COMP-THERM-027.1	1.0000(11)	1.00418(11)	1.00338(12)

Appendix B – Calculated Benchmark k_{eff} Overview

Criticality calculations have been performed for nearly one thousand ICSBEP benchmarks as part of the ENDF/B-VII.1 cross section validation and verification process. Although only a subset of these benchmark results have been discussed in detail in this paper, we tabulate the model eigenvalue and both ENDF/B-VII.0 and ENDF/B-VII.1 calculated eigenvalues for all of these systems below. Calculated values given to 5 significant figures represent 50 million neutron history (or more) calculations and have a typical stochastic uncertainty of 15 pcm or less; values given to 4 significant digits were typically run for several, but less than ten, million neutron histories and have a stochastic uncertainty of 250 pcm or less. Model uncertainties are typically several hundred pcm, although values approaching 1000 pcm or less than 100 pcm are sometimes reported. The reader should consult the

ICSBEP Handbook for more details. This Handbook was first released in the mid-1990s with annual updates since then. The models used herein come from the 2005 or later editions.

Table B1. Model and calculated eigenvalues for selected ICSBEP benchmarks

Benchmark	Model	VII.0	VII.1
HEU-MET-FAST-001	1.000	0.99984	0.99980
HEU-MET-FAST-002	1.000	1.00225	1.00239
	1.000	1.00035	1.00050
	1.000	0.99972	0.99976
	1.000	1.00004	0.99994
	1.000	1.00121	1.00131
HEU-MET-FAST-003	1.000	0.99505	0.99490
	1.000	0.99457	0.99441
	1.000	0.99918	0.99909
	1.000	0.99733	0.99721
	1.000	1.00139	1.00133
	1.000	1.00193	1.00176
	1.000	1.00190	1.00210
	1.000	1.00836	1.00137
	1.000	1.00927	1.00177
	1.000	1.01262	1.00518
	1.000	1.01677	1.00980
	1.000	1.00837	1.00874
HEU-MET-FAST-004	1.0020	1.00314	1.00307
HEU-MET-FAST-005	1.0000	0.99551	0.99519
	1.0007	0.99571	0.99792
	0.9996	0.99668	1.00051
	0.9989	0.99002	0.99448
	0.9980	0.99634	0.99912
	0.9987	0.99598	0.99779
HEU-MET-FAST-007	0.9950	0.99314	0.99290
	0.9964	0.99877	0.99886
	0.9990	1.00022	1.00029
	0.9948	0.99812	0.99830
	0.9978	1.00035	1.00015
	1.0006	1.00567	1.00582
	0.9974	1.00128	1.00146
	0.9973	0.99945	0.99937
	0.9995	1.00340	1.00327
	0.9981	0.99917	0.99922
	0.9958	0.99798	0.99769
	0.9932	0.99306	0.99296
	0.9990	1.00050	1.00100
	0.9964	0.99712	0.99704
	0.9959	0.99672	0.99657
	0.9969	0.99763	0.99762
	0.9953	0.99607	0.99589
	0.9972	0.99864	0.99822
	0.9956	0.99689	0.99664
	0.9950	0.99811	0.99799
	0.9956	0.99912	0.99881
	0.9963	0.99960	0.99976
	0.9962	0.99949	0.99922
	0.9970	0.99990	0.99950
	0.9959	0.99865	0.99837
	0.9966	0.99854	0.99846
	1.0003	1.00252	1.00216
	0.9999	1.00373	1.00335
	0.9988	1.00178	1.00184
	1.0000	1.00282	1.00269
	1.0018	1.00481	1.00482
	1.0013	1.00607	1.00616
	0.9994	1.00099	1.00091
	1.0016	1.00303	1.00301
	0.9998	1.00082	1.00058
HEU-MET-FAST-008	0.9989	0.99586	0.99588
HEU-MET-FAST-009	0.9992	0.99503	0.99754
	0.9992	0.99541	0.99656
HEU-MET-FAST-010	0.9992	0.99744	0.99851
	0.9992	0.99740	0.99786
HEU-MET-FAST-011	0.9989	0.99915	0.99893
HEU-MET-FAST-012	0.9992	0.99835	0.99817
HEU-MET-FAST-013	0.9990	0.99745	0.99741
HEU-MET-FAST-014	0.9989	0.99774	0.99769
HEU-MET-FAST-015	0.9996	0.99470	0.99449
HEU-MET-FAST-016	0.9996	0.99868	1.00155
	0.9996	1.00136	1.00236
HEU-MET-FAST-017	0.9993	0.99715	1.00063
HEU-MET-FAST-018	1.0000	1.00016	1.00026
HEU-MET-FAST-019	1.0000	1.00708	1.00718
HEU-MET-FAST-020	1.0000	1.00087	1.00070
HEU-MET-FAST-021	1.0000	0.99748	0.99719
HEU-MET-FAST-022	1.0000	0.99769	0.99766
HEU-MET-FAST-024	0.9990	0.99859	0.99824
HEU-MET-FAST-025	0.9987	0.99811	0.99901
	0.9990	1.00002	1.00119
	0.9991	1.00247	1.00388
	0.9995	1.00448	1.00540
	0.9991	1.00459	1.00532
HEU-MET-FAST-026	1.0000		1.0032
HEU-MET-FAST-027	1.0000	1.00070	1.00076
HEU-MET-FAST-028	1.0000	1.00297	1.00298
HEU-MET-FAST-029	1.0000	1.00566	1.00577
HEU-MET-FAST-030	1.0000	0.99906	1.00203
HEU-MET-FAST-031	1.0000	1.00526	1.00495
HEU-MET-FAST-032	1.0000	1.00436	1.00429
	1.0000	1.00485	1.00473
	1.0000	1.00015	1.00029
	1.0000	1.00112	1.00087
HEU-MET-FAST-033	0.9991	0.99908	0.99903
	0.9991	0.99757	0.99763
HEU-MET-FAST-034	0.9990	0.99950	0.99699
	0.9990	0.99849	0.99876
	0.9990	0.99743	0.99726
HEU-MET-FAST-036	0.9993	0.99885	0.99874
	0.9993	0.99840	0.99817
HEU-MET-FAST-037	0.9997	1.00233	1.00231
	0.9997	0.99805	0.99797
HEU-MET-FAST-038	0.9999	1.00049	1.00304
	0.9999	1.00048	1.00201
HEU-MET-FAST-040	0.9991	1.00310	1.00436
HEU-MET-FAST-041	1.0013	1.00279	1.00682
	1.0022	1.00024	1.00522

Benchmark	Model	VII.0	VII.1
	1.0006	1.00234	1.00252
	1.0006	1.00732	1.00727
	1.0006	1.00300	1.00302
	1.0006	1.00428	1.00428
HEU-MET-FAST-043	0.9995	0.99905	0.99914
	0.9995	0.99737	0.99811
	0.9995	0.99866	0.99875
	0.9995	0.99810	0.99725
	0.9995	0.99905	0.99842
HEU-MET-FAST-044	0.9995	0.99999	1.00010
	0.9995	0.99958	0.99937
	0.9995	0.99980	0.99987
	0.9995	0.99946	0.99933
	0.9995	1.00000	1.00007
HEU-MET-FAST-047	1.0007	1.00166	1.00213
HEU-MET-FAST-049	0.9990	0.99986	0.99799
	0.9994	1.00356	0.99961
	0.9994	1.00420	0.99844
HEU-MET-FAST-051	0.9971	0.99512	0.99494
	0.9968	0.99555	0.99551
	0.9974	0.99505	0.99502
	0.9969	0.99527	0.99508
	0.9982	0.99487	0.99485
	0.9996	0.99884	0.99868
	0.9998	0.99810	0.99777
	0.9981	0.99642	0.99635
	0.9969	0.99551	0.99552
	0.9984	0.99388	0.99404
HEU-MET-FAST-055	0.9955	0.99876	0.99832
	1.0013	1.00396	1.00343
HEU-MET-FAST-057	1.0000	0.98933	0.98964
	1.0000	0.99804	0.99830
	1.0000	1.01703	1.01735
	1.0000	0.98781	0.98779
	1.0000	1.02149	1.02178
	1.0000	0.99652	0.99679
HEU-MET-FAST-058	1.0000	0.99971	1.00345
	1.0000	1.00001	1.00505
	1.0000	0.99848	1.00300
	1.0000	0.99841	1.00206
	1.0000	0.99810	1.00093
HEU-MET-FAST-060	0.9955	1.01563	1.00268
	1.0013	1.02070	1.00848
HEU-MET-FAST-061	0.9998	1.00618	1.00502
	1.0006	1.00431	1.00257
HEU-MET-FAST-063	0.9993	1.00079	1.00052
	0.9988	1.00073	1.00093
HEU-MET-FAST-064	0.9996	0.99514	0.99538
	0.9996	0.99525	0.99567
	0.9996	0.99326	0.99366
HEU-MET-FAST-065	0.9995	0.99810	0.99802
HEU-MET-FAST-066	1.0030	0.99797	1.00344
	1.0023	0.99670	1.00159
	1.0023	1.00013	1.00465
	1.0043	0.99935	1.00509
	1.0030	0.99831	1.00429
	1.0028	0.99804	1.00355
	1.0048	0.99937	1.00553

Benchmark	Model	VII.0	VII.1
	1.0039	0.99873	1.00457
	1.0027	0.99641	1.00275
HEU-MET-FAST-067	0.9959	1.00936	1.00291
	1.0023	1.01604	1.00852
HEU-MET-FAST-072	1.0000	1.00890	1.00874
HEU-MET-FAST-073	1.0004	1.01148	1.01134
HEU-MET-FAST-077	1.0001	0.99513	1.00077
	0.9995	0.99583	1.00067
	0.9995	0.99325	0.99800
	0.9998	0.99310	0.99854
	0.9994	0.99469	1.00002
	0.9996	0.99430	0.99976
	0.9994	0.99587	1.00065
	0.9994	0.99251	0.99836
HEU-MET-FAST-078	0.9995	0.99474	0.99450
	0.9994	0.99610	0.99607
	0.9991	0.99626	0.99634
	1.0000	0.99864	0.99860
	0.9997	0.99588	0.99553
	0.9995	0.99589	0.99587
	1.0000	0.99731	0.99726
	0.9991	0.99670	0.99663
	0.9995	0.99655	0.99631
	0.9992	0.99814	0.99799
	0.9992	0.99760	0.99742
	0.9992	0.99602	0.99596
	1.0000	1.00218	1.00241
	0.9994	0.99507	0.99516
	0.9996	0.99615	0.99599
	0.9991	0.99438	0.99442
	0.9986	0.99646	0.99623
	0.9989	0.99680	0.99673
	0.9992	0.99685	0.99675
	1.0000	0.99761	0.99766
HEU-MET-FAST-079	0.9996	1.00105	0.99965
	0.9996	1.00114	0.99914
	0.9996	1.00339	1.00008
	0.9996	1.00513	1.00094
	0.9996	1.00413	0.99988
HEU-MET-FAST-082	0.9992	0.99647	0.99632
	0.9989	0.99611	0.99601
	0.9989	0.99846	0.99841
HEU-MET-FAST-084	0.9994	0.99908	0.99904
	0.9994	0.99948	0.99940
	0.9993	0.99686	1.00000
	0.9994	0.99873	0.99886
	0.9993	1.00513	1.00518
	0.9994	0.99872	0.99874
	0.9995	0.99753	0.99754
	0.9994	1.00833	1.00835
	0.9993	1.00278	1.00267
	0.9993	1.00137	1.00110
	0.9995	1.00148	1.00145
	0.9994	1.00324	0.99734
	0.9994	0.99914	0.99904
	0.9994	1.00540	0.99961
	0.9995	0.99801	0.99807
	0.9994	0.99744	0.99899

Benchmark	Model	VII.0	VII.1
	0.9995	1.00035	1.00054
	0.9995	0.99768	0.99768
	0.9996	0.99750	0.99747
	0.9995	1.00300	1.00278
	0.9995	1.00024	1.00024
	0.9994	0.99827	0.99833
	0.9993	0.99957	0.99950
	0.9996	0.99884	0.99878
	0.9995	1.00149	0.99824
	0.9993	0.99840	1.00043
	0.9994	0.99547	0.99768
HEU-MET-FAST-085	0.9998	1.00038	0.99992
	0.9997	1.00442	1.00442
	0.9995	0.99622	0.99626
	0.9996	0.99643	0.99993
	0.9995	1.00071	1.00061
	0.9997	1.01383	1.00565
HEU-MET-FAST-087	0.9991	0.99859	0.99835
HEU-MET-FAST-089	0.9991	1.00012	1.00000
HEU-MET-FAST-091	0.9996	0.99962	0.99969
HEU-MET-INTER-001	0.9966	1.00802	1.00135
HEU-MET-INTER-006	0.9977	0.99295	0.99316
	1.0001	0.99712	0.99697
	1.0015	1.00082	1.00079
	1.0016	1.00737	1.00721
HEU-COMP-INTER-003	1.0000	1.00660	1.00678
	1.0000	1.00679	1.00705
	1.0000	1.00236	1.00268
	1.0000	1.00461	1.00425
	1.0000	0.99650	0.99731
	1.0000	0.00520	0.99526
	1.0000	0.99706	0.99706
HEU-MET-MIXED-001	0.9995	1.00493	1.00217
HEU-MET-MIXED-002	1.0000	1.00692	1.00669
HEU-MET-MIXED-003	1.0000	1.00774	1.00757
HEU-MET-MIXED-004	0.9999	1.00296	1.00252
HEU-MET-MIXED-015	0.9996	0.99926	0.99696
HEU-MET-MIXED-016	0.9995	1.00123	1.00171
	0.9995	1.00240	1.00250
HEU-MET-THERM-012	0.9956	1.00937	1.00918
HEU-MET-THERM-014	0.9931	1.00814	1.00802
HEU-MET-THERM-031	1.0037	1.00906	1.00824

Benchmark	Model	VII.0	VII.1
HEU-MET-THERM-033	0.9939	1.00365	1.00364
HEU-SOL-THERM-001	1.0004	0.99830	0.99794
	1.0021	0.99610	0.99595
	1.0003	1.00140	1.00193
	1.0008	0.99820	0.99841
	1.0001	0.99868	0.99871
	1.0002	1.00191	1.00202
	1.0008	0.99813	0.99793
	0.9998	0.99814	0.99803
	1.0008	0.99437	0.99428
	0.9993	0.99224	0.99243
HEU-SOL-THERM-004	1.0000	0.98577	0.98720
	1.0000	0.98126	0.98273
	1.0000	0.98803	0.98983
	1.0000	0.99051	0.99246
	1.0000	0.98887	0.99098
	1.0000	0.98580	0.98785
HEU-SOL-THERM-006	0.9973	0.98258	0.98182
	0.9986	0.98686	0.98681
	1.0000	0.99850	0.99846
	1.0000	1.00097	1.00084
	1.0000	1.00790	1.00763
	1.0000	0.99927	0.99885
	1.0000	1.00075	1.00082
	0.9973	0.98178	0.98165
	0.9986	0.98652	0.98657
	1.0000	0.99785	0.99768
	1.0000	1.00096	1.00102
	0.9973	0.98122	0.98083
	0.9986	0.98505	0.98460
	1.0000	0.99924	0.99934
	1.0000	1.00681	1.00674
	1.0000	0.99914	0.99906
	1.0000	1.00089	1.00060
	1.0000	0.99957	0.99975
	1.0000	1.00747	1.00727
	1.0000	0.99896	0.99883
	1.0000	1.00089	1.00096
	1.0000	0.99881	0.99862
	1.0000	1.00087	1.00066
	1.0000	1.00791	1.00766
HEU-SOL-THERM-009	0.9990	1.00192	1.00297
	1.0000	1.00253	1.00306
	1.0000	1.00202	1.00242
	0.9986	0.99654	0.99669
HEU-SOL-THERM-010	1.0000	1.00128	1.00147
HEU-SOL-THERM-011	1.0000	1.00460	1.00466
	1.0000	1.00062	1.00100
HEU-SOL-THERM-012	0.9999	1.00104	1.00084

Benchmark	Model	VII.0	VII.1
HEU-SOL-THERM-013	1.0012	0.99852	0.99858
	1.0007		0.9976
	1.0009		0.9941
	1.0003		0.9959
HEU-SOL-THERM-020	0.9966	0.99104	0.99294
	0.9956	0.99669	0.99825
	0.9957	1.00510	1.00705
	0.9955	1.00448	1.00639
	0.9959	1.01297	1.01495
HEU-SOL-THERM-032	1.0015	0.99932	0.99933
HEU-SOL-THERM-042	0.9957	0.99665	0.99677
	0.9965	0.99657	0.99649
	0.9994	1.00082	1.00080
	1.0000	1.00218	1.00212
	1.0000	1.00006	1.00011
	1.0000	1.00042	1.00027
	1.0000	1.00126	1.00142
	1.0000	1.00201	1.00190
HEU-SOL-THERM-043	0.9986	0.99456	0.99452
	0.9995	1.00542	1.00548
	0.9990	1.00094	1.00087
HEU-SOL-THERM-049	1.0012	0.99917	0.9996
	1.0012	0.98993	0.9912
	1.0012	0.99597	0.9986
	1.0012	0.99526	0.9996
	1.0012	0.99607	1.0035
	1.0012	1.00000	1.0052
	1.0012	1.00023	1.0054
	1.0012	0.99868	1.0041
	1.0012	0.99760	0.9978
	1.0012	0.98907	0.9898
	1.0012	0.99081	0.9928
	1.0012	0.99239	0.9969
	1.0012	0.99189	0.9982
	1.0012	0.99230	0.9982
	1.0012	0.99411	1.0006
	1.0012	0.99211	0.9987
	1.0012	0.99148	0.9984
	1.0012	0.99360	0.9998
	1.0012	0.99388	1.0014
	1.0012	0.99184	0.9993
HEU-SOL-THERM-050	0.9953	1.00778	1.00835
	0.9987	1.00274	1.00339
	0.9984	1.00480	1.00626
	0.9987	1.00449	1.00513
	0.9985	1.00073	1.00124
	0.9985	1.00907	1.01019
	0.9978	0.99817	0.99966
	0.9975	0.99797	0.99885
	0.9966	0.99704	0.99842
	0.9960	0.97979	0.98076
	0.9964	0.99142	0.99173

Benchmark	Model	VII.0	VII.1
IEU-MET-FAST-001	0.9989		1.0007
	0.9997		1.0005
	0.9993		1.0012
	1.0002		1.0016
IEU-MET-FAST-002	1.000	0.99914	0.99883
IEU-MET-FAST-003	1.0000	1.00228	1.00235
IEU-MET-FAST-004	1.0000	1.00755	1.00752
IEU-MET-FAST-005	1.0000	1.00196	1.00171
IEU-MET-FAST-006	1.0000	0.99616	0.99622
IEU-MET-FAST-007	1.0045	1.00456	1.00440
	1.0045	1.00445	1.00440
	0.9948	0.99485	0.99502
IEU-MET-FAST-008	1.0000	1.00557	1.00516
IEU-MET-FAST-009	1.0000	1.01050	1.01054
IEU-MET-FAST-010	0.9954	0.99647	0.99624
	1.0014	1.00287	1.00266
IEU-MET-FAST-012	1.0007	1.00348	1.00329
	1.0014	1.00325	1.00294
IEU-MET-FAST-013	0.9941	0.99721	0.99721
	1.0022	1.00433	1.00410
IEU-COMP-FAST-001	0.9939	0.99319	0.99285
	1.0017	0.99824	0.99486
IEU-COMP-THERM-002	1.0017		1.0049
LEU-MET-THERM-002	1.0000	1.01386	1.10457
LEU-COMP-THERM-001	0.9998	0.99987	0.99964
	0.9998	0.99923	0.99913
	0.9998	0.99881	0.99848
	0.9998	0.99938	0.99932
	0.9998	0.99720	0.99701
	0.9998	0.99917	0.99901
	0.9998	0.99837	0.99833
	0.9998	0.99748	0.99734
LEU-COMP-THERM-002	0.9997	0.99854	0.99865
	0.9997	0.99975	0.99997
	0.9997	0.99922	0.99932
	0.9997	0.99902	0.99873
	0.9997	0.99801	0.99776
LEU-COMP-THERM-006	1.000	1.00003	1.00004
	1.000	1.00047	1.00034
	1.000	1.00029	1.00034
	1.000	1.00035	0.99989
	1.000	0.99990	0.99981
	1.000	1.00035	1.00031
	1.000	1.00006	1.00005
	1.000	0.99992	1.00004
	1.000	1.00012	1.00003
	1.000	0.99988	0.99978

Benchmark	Model	VII.0	VII.1
	1.000	0.99994	0.99991
	1.000	0.99983	0.99965
	1.000	0.99957	0.99954
	1.000	1.00016	0.99952
	1.000	0.99983	0.99981
	1.000	0.99985	0.99971
	1.000	0.99957	0.99975
	1.000	0.99981	0.99961
LEU-COMP-THERM-007	1.0000	0.99763	0.99761
	1.0000	0.99890	0.99880
	1.0000	0.99790	0.99766
	1.0000	0.99836	0.99813
	1.0000	0.99710	0.99714
	1.0000	0.99911	0.99883
	1.0000	0.99874	0.99834
	1.0000	0.99853	0.99822
	1.0000	0.99855	0.99814
	1.0000	0.99886	0.99850
LEU-COMP-THERM-008	1.0007	1.00091	1.00098
	1.0007	1.00118	1.00115
	1.0007	1.00146	1.00154
	1.0007	1.00087	1.00085
	1.0007	1.00011	1.00091
	1.0007	1.00074	1.00093
	1.0007	1.00070	1.00051
	1.0007	0.99968	1.00007
	1.0007	1.00035	1.00007
	1.0007	1.00073	1.00065
	1.0007	1.00164	1.00160
	1.0007	1.00110	1.00085
LEU-COMP-THERM-010	1.0000	1.00571	1.00486
	1.0000	1.00585	1.00518
	1.0000	1.00489	1.00403
	1.0000	0.99703	0.99689
	1.0000	0.99943	0.99984
	1.0000	1.00012	1.00021
	1.0000	1.00102	1.00142
	1.0000	0.99807	0.99816
	1.0000	0.99992	0.99977
	1.0000	1.00055	1.00002
	1.0000	1.00063	1.00024
	1.0000	0.99988	0.99966
	1.0000	0.99776	0.99761
LEU-COMP-THERM-011	1.0000	0.99865	0.99876
	1.0000	0.99831	0.99839
	1.0000	0.99855	0.99858
	1.0000	0.99842	0.99838
	1.0000	0.99640	0.99644
LEU-COMP-THERM-017	1.0000	1.00185	1.00157
	1.0000	1.00179	1.00121
	1.0000	1.00034	0.99959
	1.0000	0.99810	0.99810
	1.0000	0.99985	0.99989

Benchmark	Model	VII.0	VII.1
	1.0000	1.00022	1.00005
	1.0000	0.99990	1.00021
	1.0000	0.99860	0.99845
	1.0000	0.99767	0.99777
	1.0000	0.99838	0.99824
	1.0000	0.99852	0.99841
	1.0000	0.99878	0.99849
	1.0000	0.99891	0.99894
	1.0000	0.99931	0.99922
LEU-COMP-THERM-022	1.0000	1.00289	1.00270
	1.0000	1.00701	1.00707
	1.0000	1.00739	1.00797
	1.0000	1.00814	1.00827
	1.0000	1.00344	1.00347
	1.0000	1.00148	1.00163
	1.0000	1.00399	1.00404
LEU-COMP-THERM-024	1.0000	1.00131	1.00133
	1.0000	1.00842	1.00876
LEU-COMP-THERM-025	1.0000	0.98829	0.98835
	1.0000	0.99563	0.99571
	1.0000	1.00027	1.00054
	1.0000	1.00236	1.00276
LEU-COMP-THERM-027	1.0014	1.00519	1.00418
	1.0014	1.00735	1.00672
	1.0014	1.00790	1.00720
	1.0014		1.00937
LEU-COMP-THERM-035	1.0000	0.99995	0.99998
	1.0000	0.99919	0.99900
	1.0000	0.99537	0.99767
LEU-COMP-THERM-039	1.0000	0.99742	0.99722
	1.0000	0.99827	0.99796
	1.0000	0.99744	0.99724
	1.0000	0.99647	0.99635
	1.0000	0.99787	0.99769
	1.0000	0.99746	0.99729
	1.0000	0.99725	0.99681
	1.0000	0.99718	0.99719
	1.0000	0.99689	0.99691
	1.0000	0.99768	0.99742
LEU-SOL-THERM-002	1.0038		0.9998
	1.0024		0.9957
LEU-SOL-THERM-004	0.9994	1.00038	1.00040
	0.9999	1.00153	1.00182
	0.9999	0.99973	0.99959
	0.9999	1.00203	1.00217
	0.9999	1.00197	1.00200
	0.9994	1.00128	1.00106
	0.9996	1.00142	1.00138
LEU-SOL-THERM-007	0.9961	0.99497	0.99507

Benchmark	Model	VII.0	VII.1
	0.9973	0.99728	0.99724
	0.9985	0.99614	0.99630
	0.9988	0.99872	0.99889
	0.9983	0.99745	0.99742
LEU-SOL-THERM-020	0.9995	0.99991	0.99992
	0.9996	0.99974	0.99970
	0.9997	0.99896	0.99900
	0.9998	0.99982	1.00008
LEU-SOL-THERM-021	0.9983	0.99772	0.99772
	0.9985	0.99833	0.99824
	0.9989	0.99754	0.99765
	0.9993	0.99957	0.99948
PU-MET-FAST-001	1.000	0.99996	0.99988
PU-MET-FAST-002	1.000	1.00000	1.00002
PU-MET-FAST-003	1.000		0.9986
PU-MET-FAST-005	1.0000	1.00940	1.00089
PU-MET-FAST-006	1.0000	1.00123	1.00097
PU-MET-FAST-008	1.0000	0.99814	0.99770
	1.0000		0.99836
PU-MET-FAST-009	1.0000	1.00498	1.00505
PU-MET-FAST-010	1.0000	0.99974	0.99942
PU-MET-FAST-011	1.000	1.00012	1.00011
PU-MET-FAST-018	1.0000	0.99657	0.99939
PU-MET-FAST-019	0.9992	0.99795	1.00086
PU-MET-FAST-020	0.9993	0.99801	0.99812
PU-MET-FAST-021	1.0000	0.99161	1.0042
	1.0000	0.99284	0.9939
PU-MET-FAST-022	1.0000	0.99846	0.99831
PU-MET-FAST-023	1.0000	0.99989	0.99981
PU-MET-FAST-024	1.0000	1.00187	1.00188
PU-MET-FAST-025	1.0000	0.99887	0.99869
PU-MET-FAST-026	1.0000	0.99853	0.99859
PU-MET-FAST-027	1.0000	1.00294	1.00288
PU-MET-FAST-028	1.0000	0.99913	0.99917
PU-MET-FAST-029	1.0000	0.99555	0.99574
PU-MET-FAST-030	1.0000	1.00284	1.00272
PU-MET-FAST-031	1.0000	1.00440	1.00433
PU-MET-FAST-032	1.0000	0.99851	0.99859
PU-MET-FAST-033	0.9967	0.99843	0.99681
	1.0023	1.00266	1.00097
PU-MET-FAST-035	1.0000	0.99782	0.99774
PU-MET-FAST-036	1.0000	1.00645	1.00651
PU-MET-FAST-039	1.0000	0.99231	0.99230
PU-MET-FAST-040	1.0000	0.99670	0.99671
PU-MET-FAST-041	1.0000	1.00594	1.00569
PU-MET-FAST-044	0.9977	1.00535	1.00532
	0.9980	0.99995	1.00001
	0.9977	0.99788	0.99952
	0.9979	0.99991	0.99997
	0.9977	0.99909	0.99935
PU-MET-FAST-045	1.0000	0.99984	1.00114
	1.0000	1.01142	1.01251
	1.0000	1.00644	1.00765
	1.0000	1.00901	1.01016
	1.0000	1.00520	1.00643

Benchmark	Model	VII.0	VII.1
	1.0000	1.01279	1.01480
	1.0000	1.00559	1.00697
	1.0000	1.01279	1.01379
	1.0000	1.00638	1.00722
	1.0000	1.00507	1.00599
	1.0000	1.00427	1.00502
PU-MET-INTER-002	1.0016	1.02699	1.01481
PU-COMP-INTER-001	1.0000		1.0115
PU-SOL-THERM-001	1.0000	1.00566	1.00612
	1.0000	1.00747	1.00761
	1.0000	1.01067	1.01049
	1.0000	1.00484	1.00443
	1.0000	1.00868	1.00863
	1.0000	1.00955	1.00957
PU-SOL-THERM-002	1.0000	1.00386	1.00397
	1.0000	1.00474	1.00477
	1.0000	1.00378	1.00363
	1.0000	1.00653	1.00647
	1.0000	1.00917	1.00923
	1.0000	1.00524	1.00535
	1.0000	1.00739	1.00773
PU-SOL-THERM-003	1.0000	1.00257	1.00264
	1.0000	1.00217	1.00259
	1.0000	1.00495	1.00497
	1.0000	1.00451	1.00423
	1.0000	1.00532	1.00573
	1.0000	1.00573	1.00590
	1.0000	1.00665	1.00694
	1.0000	1.00559	1.00552
PU-SOL-THERM-004	1.0000	1.00389	1.00399
	1.0000	0.99870	0.99878
	1.0000	1.00066	1.00092
	1.0000	0.99871	0.99882
	1.0000	0.99971	0.99995
	1.0000	1.00152	1.00164
	1.0000	1.00558	1.00551
	1.0000	1.00127	1.00121
	1.0000	1.00044	1.00079
	1.0000	1.00229	1.00209
	1.0000	1.00044	1.00052
	1.0000	1.00320	1.00290
	1.0000	1.00025	1.00024
PU-SOL-THERM-005	1.0000	1.00226	1.00239
	1.0000	1.00268	1.00303
	1.0000	1.00337	1.00356
	1.0000	1.00498	1.00545
	1.0000	1.00628	1.00643
	1.0000	1.00585	1.00577
	1.0000	1.00418	1.00417

Benchmark	Model	VII.0	VII.1
	1.0000	0.99919	0.99949
	1.0000	1.00208	1.00220
PU-SOL-THERM-006	1.0000	1.00058	1.00051
	1.0000	1.00171	1.00211
	1.0000	1.00145	1.00155
PU-SOL-THERM-007	1.0000	1.00927	1.00951
	1.0000	1.00367	1.00392
	1.0000	1.00934	1.00939
	1.0000	1.00330	1.00321
	1.0000	1.00531	1.00528
	1.0000	0.99839	0.99891
	1.0000	0.99721	0.99722
	1.0000	1.00110	1.00089
PU-SOL-THERM-009	1.0000	1.01920	1.01928
PU-SOL-THERM-010	1.0000	1.01790	1.01820
	1.0000	1.01456	1.01473
	1.0000	1.00846	1.00815
	1.0000	1.01236	1.01263
	1.0000	1.01018	1.01036
	1.0000	1.00927	1.00945
	1.0000	1.00248	1.00256
	1.0000	1.00377	1.00366
	1.0000	1.01500	1.01481
	1.0000	1.00279	1.00289
	1.0000	1.00984	1.01002
	1.0000	1.00954	1.00961
	1.0000	1.01589	1.01591
	1.0000	1.00951	1.00960
PU-SOL-THERM-011	1.0000	1.00990	1.01020
	1.0000	1.01477	1.01475
	1.0000	1.01694	1.01654
	1.0000	1.00929	1.00949
	1.0000	1.00630	1.00628
	1.0000	0.99427	0.99462
	1.0000	1.00041	1.00050
	1.0000	0.99697	0.99702
	1.0000	0.99362	0.99377
	1.0000	1.00342	1.00340
	1.0000	1.00005	1.00024
	1.0000	0.99959	0.99971
PU-SOL-THERM-012	1.0000	1.00560	1.00542
	1.0000	1.00640	1.00598
	1.0000	1.00762	1.00731
	1.0000	1.00768	1.00769
	1.0000	1.00977	1.00990
	1.0000	1.00700	1.00681
	1.0000	1.00576	1.00561
	1.0000	1.00514	1.00414
	1.0000	1.00996	1.01003
	1.0000	1.00440	1.00426
	1.0000	1.00697	1.00668
	1.0000	1.00711	1.00698

Benchmark	Model	VII.0	VII.1
	1.0000	1.00977	1.00969
PU-SOL-THERM-018	1.0000	1.00883	1.00885
	1.0000	1.01205	1.01224
	1.0000	1.00994	1.00965
	1.0000	1.00775	1.00809
	1.0000	1.00665	1.00685
	1.0000	1.00502	1.00511
	1.0000	1.00422	1.00421
	1.0000	1.00400	1.00382
	1.0000	1.00244	1.00239
PU-SOL-THERM-021	1.0000		1.0056
	1.0000		1.0056
PU-SOL-THERM-022	1.0000	1.00006	0.99960
	1.0000	1.00263	1.00213
	1.0000	1.00132	1.00111
	1.0000	1.00166	1.00135
	1.0000	1.00250	1.00223
	1.0000	1.00296	1.00283
	1.0000	1.00457	1.00438
	1.0000	1.00511	1.00498
	1.0000	1.00371	1.00382
PU-SOL-THERM-028	1.0000	1.00795	1.00790
	1.0000	1.00739	1.00735
	1.0000	1.00905	1.00925
	1.0000	1.00879	1.00895
	1.0000	1.00987	1.00996
	1.0000	1.01081	1.01084
	1.0000	1.00821	1.00795
	1.0000	1.00808	1.00829
	1.0000	1.00997	1.01016
PU-SOL-THERM-032	1.0000	0.99613	0.99613
	1.0000	1.00168	1.00156
	1.0000	1.00289	1.00246
	1.0000	1.00250	1.00243
	1.0000	1.00448	1.00413
	1.0000	1.00447	1.00454
	1.0000	1.00501	1.00516
	1.0000	1.00454	1.00456
	1.0000	1.00320	1.00339
	1.0000	1.00495	1.00518
	1.0000	1.00439	1.00477
	1.0000	1.00327	1.00355
	1.0000	1.00214	1.00227
	1.0000	1.00196	1.00175
	1.0000	1.00391	1.00417
	1.0000	1.00379	1.00379
	1.0000	1.00383	1.00408
PU-SOL-THERM-034	1.0000	1.00033	0.99970
	1.0000	1.00167	1.00695
	1.0000	0.99935	1.00750
	1.0000	1.00240	1.01237
	1.0000	0.99994	1.01074

Benchmark	Model	VII.0	VII.1
	1.0000	1.00147	1.01265
	1.0000	0.99903	1.00335
	1.0000	0.99948	1.00397
	1.0000	0.99824	1.00291
	1.0000	0.99741	1.00266
	1.0000	0.99922	1.00423
	1.0000	0.99864	1.00399
	1.0000	0.99762	1.00245
	1.0000	0.99730	1.00261
	1.0000	0.99785	1.00313
U233-MET-FAST-001	1.0000	0.99964	0.99989
U233-MET-FAST-002	1.0000	0.99907	0.99899
	1.0000	1.00050	1.00018
U233-MET-FAST-003	1.0000	0.99450	0.99922
	1.0000	1.00016	0.99967
U233-MET-FAST-004	1.0000	1.00459	0.99862
	1.0000	1.00500	0.99536
U233-MET-FAST-005	1.0000	0.99427	0.99625
	1.0000	0.99248	0.99562
U233-MET-FAST-006	1.0000	0.99928	0.99888
U233-SOL-INTER-001	1.0000	0.98453	0.98616
	1.0000	0.98031	0.98180
	1.0000	0.98135	0.98304
	1.0000	0.99311	0.99457
	1.0000	0.98477	0.98624
	1.0000	0.98638	0.98791
	1.0000	0.98201	0.98380
	1.0000	0.98173	0.98305
	1.0000	0.97925	0.98129
	1.0000	0.97922	0.98077
	1.0000	0.98056	0.98206
	1.0000	0.98102	0.98241
	1.0000	0.98178	0.98321
	1.0000	0.99102	0.99249
	1.0000	0.97999	0.98140
	1.0000	0.98190	0.98255
	1.0000	0.98926	0.99065
	1.0000	0.97850	0.97999
	1.0000	0.97552	0.97721
	1.0000	0.98097	0.98213
	1.0000	0.97340	0.97475
	1.0000	0.97865	0.97998
	1.0000	0.99062	0.99194
	1.0000	0.99201	0.99343
	1.0000	0.98498	0.98644
	1.0000	0.98892	0.98990
	1.0000	0.99097	0.99220
	1.0000	0.98364	0.98455
	1.0000	0.97762	0.97873
	1.0000	0.97886	0.97968

Benchmark	Model	VII.0	VII.1
	1.0000	0.99126	0.99234
	1.0000	0.97622	0.97734
	1.0000	0.99410	0.99515
U233-SOL-THERM-001	1.0005	1.00130	1.00126
	1.0010	1.00139	1.00128
	1.0011	1.00087	1.00068
	1.0003	1.00089	1.00062
	1.0004	1.00025	1.00031
U233-SOL-THERM-005	1.0000	1.00192	1.00181
	1.0000	1.00515	1.00539
U233-SOL-THERM-008	1.0006	1.00153	1.00146
U233-SOL-THERM-009	0.9966	0.99612	0.99621
	0.9981	0.99930	0.99934
	0.9989	1.00058	1.00057
	0.9998	0.99934	0.99925
U233-SOL-THERM-012	1.0000	1.00085	1.00070
	1.0000	1.00010	0.99987
	1.0000	1.00962	1.00950
	1.0000	1.00269	1.00269
	1.0000	1.00491	1.00487
	1.0000	1.00599	1.00608
	1.0000	1.00194	1.00188
	1.0000	0.99908	0.99909
U233-SOL-THERM-013	0.9992	1.00532	1.00556
	0.9992	1.00545	1.00534
	0.9992	1.00578	1.00604
	0.9992	1.00637	1.00629
	0.9992	1.00694	1.00743
	0.9992	1.00617	1.00654
	0.9992	1.00631	1.00659
	0.9992	1.00734	1.00728
	0.9992	1.00759	1.00763
	0.9992	1.00799	1.00822
	0.9992	1.00524	1.00502
	0.9992	1.00620	1.00629
	0.9992	1.00357	1.00343
	0.9992	1.00684	1.00699
	0.9996	1.02136	1.02147
	0.9996	0.99380	0.99390
	0.9996	0.99678	0.99675
	0.9996	1.00036	1.00049
	0.9996	0.99657	0.99638
	0.9996	0.99995	0.99975
	0.9996	1.00229	1.00262
U233-SOL-THERM-015	1.0000	0.98983	0.99101
	1.0000	0.98518	0.98631
	1.0000	0.98640	0.98719
	1.0000	0.99007	0.99084
	1.0000	0.98623	0.98692
	1.0000	0.97695	0.97799
	1.0000	0.98795	0.98650

Benchmark	Model	VII.0	VII.1
	1.0000	0.97362	0.97448
	1.0000	0.96906	0.96996
	1.0000	0.99018	0.99071
	1.0000	0.99289	0.99389
	1.0000	0.99348	0.99424
	1.0000	0.99165	0.99241
	1.0000	0.99832	0.99931
	1.0000	0.98965	0.99048
	1.0000	0.98864	0.98926
	1.0000	0.99818	0.99848
	1.0000	0.97477	0.97526
	1.0000	0.97514	0.97613
	1.0000	0.99491	0.99559
	1.0000	0.99770	0.99847
	1.0000	0.99604	0.99678
	1.0000	0.99402	0.99455
	1.0000	0.99078	0.99157
	1.0000	0.99845	0.99870
	1.0000	0.99398	0.99456
	1.0000	0.99864	0.99893
	1.0000	0.99673	0.99727
	1.0000	0.99550	0.99606
	1.0000	0.99492	0.99514
	1.0000	0.99440	0.99435
U233-SOL-THERM-016	0.9987	1.00391	1.00408
	0.9983	1.00482	1.00479
	0.9992	1.00450	1.00444
	0.9993	0.99611	0.99629
	1.0008	0.99696	0.99697
	1.0011	0.99642	0.99667
	1.0000	1.00488	1.00460
	0.9992	1.00458	1.00450
	0.9992	1.00469	1.00461
	0.9993	1.00500	1.00519
	1.0000	1.00551	1.00578
	1.0000	1.00669	1.00662
	0.9994	1.01001	1.01019
	1.0000	0.99533	0.99540
	0.9988	0.99576	0.99617
	1.0000		0.99557
	1.0000	1.00976	1.00956
	1.0000	1.00965	1.00964
	1.0000	1.00988	1.00990
	0.9981	1.00042	1.00058
	0.9980	1.00571	1.00599
	0.9988	1.00375	1.00365
	0.9986	0.99924	0.99941
	0.9985	0.99990	1.00004
	0.9993	0.99951	0.99959
	0.9990	1.01074	1.01071
	0.9985	1.01249	1.01229
	0.9986	1.01258	1.01246
U233-SOL-THERM-017	0.9997	1.00447	1.00420
	1.0000	1.00045	1.00058
	1.0001	1.00533	1.00528
	0.9994	1.00565	1.00569

Benchmark	Model	VII.0	VII.1
	1.0000	1.00198	1.00210
	1.0000	1.00088	1.00076
	1.0000	1.00045	1.00036
U233-COMP-THERM-001	1.0006	1.00183	1.00166
	1.0015	1.00486	1.00464
	1.0000	1.00459	1.00421
	1.0007	1.00269	1.00270
	1.0015	1.00233	1.00193
	1.0015	1.00017	0.99994
	0.9995	1.00367	1.00308
	1.0004	1.00162	1.00106
U233-COMP-THERM-004	1.0017		0.99826
MIX-MET-FAST-001	1.0000	0.99938	0.99955
MIX-MET-FAST-002	1.0000	1.00561	1.00521
	1.0000	1.00536	1.00540
	1.0000	1.00537	1.00543
MIX-MET-FAST-003	0.9993	1.00058	1.00078
MIX-MET-FAST-004	0.9993	0.99944	1.00037
	0.9993	0.99909	0.99957
MIX-MET-FAST-005	0.9990	1.00393	1.00393
MIX-MET-FAST-007	1.0000	1.00046	1.00321
	1.0000	1.00497	1.00820
	1.0000	1.00260	1.00641
	1.0000	1.00190	1.00545
	1.0000	0.99991	1.00253
	1.0000	0.99938	1.00095
	1.0000	1.00295	1.00609
	1.0000	1.00187	1.00523
	1.0000	1.00166	1.00536
	1.0000	1.00156	1.00492
	1.0000	1.00063	1.00352
	1.0000	1.00072	1.00228
	1.0000	1.00007	1.00056
	1.0000	1.00448	1.00783
	1.0000	1.00407	1.00778
	1.0000	1.00297	1.00595
	1.0000	1.00350	1.00584
	1.0000	1.00651	1.00789
	1.0000	1.00416	1.00692
	1.0000	1.00300	1.00498
	1.0000	1.00424	1.00515
	1.0000	1.00161	1.00395
	1.0000	1.00203	1.00395
MIX-MET-FAST-009	1.0000	1.00012	1.00014
MIX-MET-FAST-010	1.0000	0.99994	0.99977
MIX-COMP-FAST-001	0.9866	0.98781	0.98563
	1.0006	1.00594	1.00346
MIX-COMP-THERM-002	1.0024		1.0008
	1.0009		1.0016
	1.0042		1.0027

Benchmark	Model	VII.0	VII.1
	1.0024		1.0064
	1.0038		1.0036
	1.0029		1.0056